

# International Journal on

# Advances in Telecommunications



2020 vol. 13 nr. 1&2

The *International Journal on Advances in Telecommunications* is published by IARIA.

ISSN: 1942-2601

journals site: <http://www.ariajournals.org>

contact: [petre@aria.org](mailto:petre@aria.org)

Responsibility for the contents rests upon the authors and not upon IARIA, nor on IARIA volunteers, staff, or contractors.

IARIA is the owner of the publication and of editorial aspects. IARIA reserves the right to update the content for quality improvements.

Abstracting is permitted with credit to the source. Libraries are permitted to photocopy or print, providing the reference is mentioned and that the resulting material is made available at no cost.

Reference should mention:

*International Journal on Advances in Telecommunications, issn 1942-2601*  
vol. 13, no. 1 & 2, year 2020, <http://www.ariajournals.org/telecommunications/>

The copyright for each included paper belongs to the authors. Republishing of same material, by authors or persons or organizations, is not allowed. Reprint rights can be granted by IARIA or by the authors, and must include proper reference.

Reference to an article in the journal is as follows:

<Author list>, "<Article title>"  
*International Journal on Advances in Telecommunications, issn 1942-2601*  
vol. 13, no. 1 & 2, year 2020, <start page>:<end page> , <http://www.ariajournals.org/telecommunications/>

IARIA journals are made available for free, proving the appropriate references are made when their content is used.

Sponsored by IARIA

[www.aria.org](http://www.aria.org)

Copyright © 2020 IARIA

**Editors-in-Chief**

Tulin Atmaca, Institut Mines-Telecom/ Telecom SudParis, France  
Marko Jääntti, University of Eastern Finland, Finland

**Editorial Advisory Board**

Ioannis D. Moscholios, University of Peloponnese, Greece  
Ilija Basicovic, University of Novi Sad, Serbia  
Kevin Daimi, University of Detroit Mercy, USA  
György Kálmán, Gjøvik University College, Norway  
Michael Massoth, University of Applied Sciences - Darmstadt, Germany  
Mariusz Glabowski, Poznan University of Technology, Poland  
Dragana Krstic, Faculty of Electronic Engineering, University of Nis, Serbia  
Wolfgang Leister, Norsk Regnesentral, Norway  
Bernd E. Wolfinger, University of Hamburg, Germany  
Przemyslaw Pochec, University of New Brunswick, Canada  
Timothy Pham, Jet Propulsion Laboratory, California Institute of Technology, USA  
Kamal Harb, KFUPM, Saudi Arabia  
Eugen Borcoci, University "Politehnica" of Bucharest (UPB), Romania  
Richard Li, Huawei Technologies, USA

**Editorial Board**

Fatma Abdelkefi, High School of Communications of Tunis - SUPCOM, Tunisia  
Seyed Reza Abdollahi, Brunel University - London, UK  
Habtamu Abie, Norwegian Computing Center/Norsk Regnesentral-Blindern, Norway  
Rui L. Aguiar, Universidade de Aveiro, Portugal  
Javier M. Aguiar Pérez, Universidad de Valladolid, Spain  
Mahdi Aiash, Middlesex University, UK  
Akbar Sheikh Akbari, Staffordshire University, UK  
Ahmed Akl, Arab Academy for Science and Technology (AAST), Egypt  
Hakiri Akram, LAAS-CNRS, Toulouse University, France  
Anwer Al-Dulaimi, Brunel University, UK  
Muhammad Ali Imran, University of Surrey, UK  
Muayad Al-Janabi, University of Technology, Baghdad, Iraq  
Jose M. Alcaraz Calero, Hewlett-Packard Research Laboratories, UK / University of Murcia, Spain  
Erick Amador, Intel Mobile Communications, France  
Ermeson Andrade, Universidade Federal de Pernambuco (UFPE), Brazil  
Cristian Anghel, University Politehnica of Bucharest, Romania  
Regina B. Araujo, Federal University of Sao Carlos - SP, Brazil  
Pasquale Ardimento, University of Bari, Italy  
Ezendu Ariwa, London Metropolitan University, UK  
Miguel Arjona Ramirez, São Paulo University, Brasil  
Radu Arsinte, Technical University of Cluj-Napoca, Romania  
Tulin Atmaca, Institut Mines-Telecom/ Telecom SudParis, France  
Mario Ezequiel Augusto, Santa Catarina State University, Brazil

Marco Aurelio Spohn, Federal University of Fronteira Sul (UFFS), Brazil  
Philip L. Balcaen, University of British Columbia Okanagan - Kelowna, Canada  
Marco Baldi, Università Politecnica delle Marche, Italy  
Ilija Basicovic, University of Novi Sad, Serbia  
Carlos Becker Westphall, Federal University of Santa Catarina, Brazil  
Mark Bentum, University of Twente, The Netherlands  
David Bernstein, Huawei Technologies, Ltd., USA  
Eugen Borcoci, University "Politehnica" of Bucharest (UPB), Romania  
Fernando Boronat Seguí, Universidad Politecnica de Valencia, Spain  
Christos Bouras, University of Patras, Greece  
Martin Brandl, Danube University Krems, Austria  
Julien Broisin, IRIT, France  
Dumitru Burdescu, University of Craiova, Romania  
Andi Buzo, University "Politehnica" of Bucharest (UPB), Romania  
Shkelzen Cakaj, Telecom of Kosovo / Prishtina University, Kosovo  
Enzo Alberto Candreva, DEIS-University of Bologna, Italy  
Rodrigo Capobianco Guido, São Paulo State University, Brazil  
Hakima Chaouchi, Telecom SudParis, France  
Silviu Ciochina, Universitatea Politehnica din Bucuresti, Romania  
José Coimbra, Universidade do Algarve, Portugal  
Hugo Coll Ferri, Polytechnic University of Valencia, Spain  
Noel Crespi, Institut TELECOM SudParis-Evry, France  
Leonardo Dagui de Oliveira, Escola Politécnica da Universidade de São Paulo, Brazil  
Kevin Daimi, University of Detroit Mercy, USA  
Gerard Damm, Alcatel-Lucent, USA  
Francescantonio Della Rosa, Tampere University of Technology, Finland  
Chérif Diallo, Consultant Sécurité des Systèmes d'Information, France  
Klaus Drechsler, Fraunhofer Institute for Computer Graphics Research IGD, Germany  
Jawad Drissi, Cameron University, USA  
António Manuel Duarte Nogueira, University of Aveiro / Institute of Telecommunications, Portugal  
Alban Duverdiere, CNES (French Space Agency) Paris, France  
Nicholas Evans, EURECOM, France  
Fabrizio Falchi, ISTI - CNR, Italy  
Mário F. S. Ferreira, University of Aveiro, Portugal  
Bruno Filipe Marques, Polytechnic Institute of Viseu, Portugal  
Robert Forster, Edgemount Solutions, USA  
John-Austen Francisco, Rutgers, the State University of New Jersey, USA  
Kaori Fujinami, Tokyo University of Agriculture and Technology, Japan  
Shauneen Furlong, University of Ottawa, Canada / Liverpool John Moores University, UK  
Emiliano Garcia-Palacios, ECIT Institute at Queens University Belfast - Belfast, UK  
Ana-Belén García-Hernando, Universidad Politécnica de Madrid, Spain  
Bezalel Gavish, Southern Methodist University, USA  
Christos K. Georgiadis, University of Macedonia, Greece  
Mariusz Glabowski, Poznan University of Technology, Poland  
Katie Goeman, Hogeschool-Universiteit Brussel, Belgium  
Hock Guan Goh, Universiti Tunku Abdul Rahman, Malaysia  
Pedro Gonçalves, ESTGA - Universidade de Aveiro, Portugal  
Valerie Gouet-Brunet, Conservatoire National des Arts et Métiers (CNAM), Paris  
Christos Grecos, University of West of Scotland, UK  
Stefanos Gritzalis, University of the Aegean, Greece  
William I. Grosky, University of Michigan-Dearborn, USA  
Vic Grout, Glyndwr University, UK  
Xiang Gui, Massey University, New Zealand

Huaqun Guo, Institute for Infocomm Research, A\*STAR, Singapore  
Song Guo, University of Aizu, Japan  
Kamal Harb, KFUPM, Saudi Arabia  
Ching-Hsien (Robert) Hsu, Chung Hua University, Taiwan  
Javier Ibanez-Guzman, Renault S.A., France  
Lamiaa Fattouh Ibrahim, King Abdul Aziz University, Saudi Arabia  
Theodoros Iliou, University of the Aegean, Greece  
Mohsen Jahanshahi, Islamic Azad University, Iran  
Antonio Jara, University of Murcia, Spain  
Carlos Juiz, Universitat de les Illes Balears, Spain  
Adrian Kacso, Universität Siegen, Germany  
György Kálmán, Gjøvik University College, Norway  
Eleni Kaplani, University of East Anglia-Norwich Research Park, UK  
Behrouz Khoshnevis, University of Toronto, Canada  
Ki Hong Kim, ETRI: Electronics and Telecommunications Research Institute, Korea  
Atsushi Koike, Seikei University, Japan  
Ousmane Kone, UPPA - University of Bordeaux, France  
Dragana Krstic, University of Nis, Serbia  
Archana Kumar, Delhi Institute of Technology & Management, Haryana, India  
Romain Laborde, University Paul Sabatier (Toulouse III), France  
Massimiliano Laddomada, Texas A&M University-Texarkana, USA  
Wen-Hsing Lai, National Kaohsiung First University of Science and Technology, Taiwan  
Zhihua Lai, Ranplan Wireless Network Design Ltd., UK  
Jong-Hyouk Lee, INRIA, France  
Wolfgang Leister, Norsk Regnesentral, Norway  
Elizabeth I. Leonard, Naval Research Laboratory - Washington DC, USA  
Richard Li, Huawei Technologies, USA  
Jia-Chin Lin, National Central University, Taiwan  
Chi (Harold) Liu, IBM Research - China, China  
Diogo Lobato Acatauassu Nunes, Federal University of Pará, Brazil  
Andreas Loeffler, Friedrich-Alexander-University of Erlangen-Nuremberg, Germany  
Michael D. Logothetis, University of Patras, Greece  
Renata Lopes Rosa, University of São Paulo, Brazil  
Hongli Luo, Indiana University Purdue University Fort Wayne, USA  
Christian Maciocco, Intel Corporation, USA  
Dario Maggiorini, University of Milano, Italy  
Maryam Tayefeh Mahmoudi, Research Institute for ICT, Iran  
Krešimir Malarić, University of Zagreb, Croatia  
Zoubir Mammeri, IRIT - Paul Sabatier University - Toulouse, France  
Herwig Mannaert, University of Antwerp, Belgium  
Michael Massoth, University of Applied Sciences - Darmstadt, Germany  
Adrian Matei, Orange Romania S.A, part of France Telecom Group, Romania  
Natarajan Meghanathan, Jackson State University, USA  
Emmanouel T. Michailidis, University of Piraeus, Greece  
Ioannis D. Moscholios, University of Peloponnese, Greece  
Djafar Mynbaev, City University of New York, USA  
Pubudu N. Pathirana, Deakin University, Australia  
Christopher Nguyen, Intel Corp., USA  
Lim Nguyen, University of Nebraska-Lincoln, USA  
Brian Niehöfer, TU Dortmund University, Germany  
Serban Georgica Obreja, University Politehnica Bucharest, Romania  
Peter Orosz, University of Debrecen, Hungary  
Patrik Österberg, Mid Sweden University, Sweden

Harald Øverby, ITEM/NTNU, Norway  
Tudor Palade, Technical University of Cluj-Napoca, Romania  
Constantin Paleologu, University Politehnica of Bucharest, Romania  
Stelios Papaharalabos, National Observatory of Athens, Greece  
Gerard Parr, University of Ulster Coleraine, UK  
Ling Pei, Finnish Geodetic Institute, Finland  
Jun Peng, University of Texas - Pan American, USA  
Cathryn Peoples, University of Ulster, UK  
Dionysia Petraki, National Technical University of Athens, Greece  
Dennis Pfisterer, University of Luebeck, Germany  
Timothy Pham, Jet Propulsion Laboratory, California Institute of Technology, USA  
Roger Pierre Fabris Hoefel, Federal University of Rio Grande do Sul (UFRGS), Brazil  
Przemyslaw Pochec, University of New Brunswick, Canada  
Anastasios Politis, Technological & Educational Institute of Serres, Greece  
Adrian Popescu, Blekinge Institute of Technology, Sweden  
Neeli R. Prasad, Aalborg University, Denmark  
Dušan Radović, TES Electronic Solutions, Stuttgart, Germany  
Victor Ramos, UAM Iztapalapa, Mexico  
Gianluca Reali, Università degli Studi di Perugia, Italy  
Eric Renault, Telecom SudParis, France  
Leon Reznik, Rochester Institute of Technology, USA  
Joel Rodrigues, Instituto de Telecomunicações / University of Beira Interior, Portugal  
David Sánchez Rodríguez, University of Las Palmas de Gran Canaria (ULPGC), Spain  
Panagiotis Sarigiannidis, University of Western Macedonia, Greece  
Michael Sauer, Corning Incorporated, USA  
Marialisa Scatà, University of Catania, Italy  
Zary Segall, Chair Professor, Royal Institute of Technology, Sweden  
Sergei Semenov, Broadcom, Finland  
Dimitrios Serpanos, University of Patras and ISI/RC Athena, Greece  
Adão Silva, University of Aveiro / Institute of Telecommunications, Portugal  
Pushpendra Bahadur Singh, MindTree Ltd, India  
Mariusz Skrocki, Orange Labs Poland / Telekomunikacja Polska S.A., Poland  
Leonel Sousa, INESC-ID/IST, TU-Lisbon, Portugal  
Cristian Stanciu, University Politehnica of Bucharest, Romania  
Liana Stanescu, University of Craiova, Romania  
Cosmin Stoica Spahiu, University of Craiova, Romania  
Young-Joo Suh, POSTECH (Pohang University of Science and Technology), Korea  
Hailong Sun, Beihang University, China  
Jani Suomalainen, VTT Technical Research Centre of Finland, Finland  
Fatma Tansu, Eastern Mediterranean University, Cyprus  
Ioan Toma, STI Innsbruck/University Innsbruck, Austria  
Božo Tomas, HT Mostar, Bosnia and Herzegovina  
Piotr Tyczka, ITTI Sp. z o.o., Poland  
John Vardakas, University of Patras, Greece  
Andreas Veglis, Aristotle University of Thessaloniki, Greece  
Luís Veiga, Instituto Superior Técnico / INESC-ID Lisboa, Portugal  
Calin Vladeanu, "Politehnica" University of Bucharest, Romania  
Benno Volk, ETH Zurich, Switzerland  
Krzysztof Walczak, Poznan University of Economics, Poland  
Krzysztof Walkowiak, Wroclaw University of Technology, Poland  
Yang Wang, Georgia State University, USA  
Yean-Fu Wen, National Taipei University, Taiwan, R.O.C.  
Bernd E. Wolfinger, University of Hamburg, Germany

Riaan Wolhuter, Universiteit Stellenbosch University, South Africa  
Yulei Wu, Chinese Academy of Sciences, China  
Mudasser F. Wyne, National University, USA  
Gaoxi Xiao, Nanyang Technological University, Singapore  
Bashir Yahya, University of Versailles, France  
Abdulrahman Yarali, Murray State University, USA  
Mehmet Erkan Yüksel, Istanbul University, Turkey  
Pooneh Bagheri Zadeh, Staffordshire University, UK  
Giannis Zaoudis, University of Patras, Greece  
Liaoyuan Zeng, University of Electronic Science and Technology of China, China  
Rong Zhao , Detecon International GmbH, Germany  
Zhiwen Zhu, Communications Research Centre, Canada  
Martin Zimmermann, University of Applied Sciences Offenburg, Germany  
Piotr Zwierzykowski, Poznan University of Technology, Poland

**CONTENTS**

*pages: 1 - 9*

**Evaluation of the Complexity, Performance and Implementability of Geometrical MIMO Detectors: the Example of the Exploration and Exploitation List Detector**

Bastien Trotobas, SCEE/IETR UMR CNRS 6164, CentraleSupélec, France

Youness Akourim, École normale supérieure de Rennes, France

Amor Nafkha, SCEE/IETR UMR CNRS 6164, CentraleSupélec, France

Yves Louët, SCEE/IETR UMR CNRS 6164, CentraleSupélec, France

Jacques Weiss, CentraleSupélec, France

*pages: 10 - 20*

**AI Based Beam Management for 5G (mmWave) at Wireless Edge**

Chitwan Arora, Hughes Systique Corporation, Gurgaon, India

Abheek Saha, Hughes Systique Corporation, Gurgaon, India

# Evaluation of the Complexity, Performance and Implementability of Geometrical MIMO Detectors: the Example of the Exploration and Exploitation List Detector

Bastien Trotobas\*, Youness Akourim<sup>†</sup>, Amor Nafkha\*, Yves Louët\* and Jacques Weiss<sup>‡</sup>

\*SCEE/IETR UMR CNRS 6164, CentraleSupélec

Avenue de la boulaie, 35576 Cesson Sévigné, France

Email: [bastien.trotobas@centralesupelec.fr](mailto:bastien.trotobas@centralesupelec.fr)

[amor.nafkha@centralesupelec.fr](mailto:amor.nafkha@centralesupelec.fr)

[yves.louet@centralesupelec.fr](mailto:yves.louet@centralesupelec.fr)

<sup>†</sup>École normale supérieure de Rennes

Campus de Ker Lann, Avenue Robert Schuman, 35170 Bruz, France

Email: [youness.akourim@ens-rennes.fr](mailto:youness.akourim@ens-rennes.fr)

<sup>‡</sup>CentraleSupélec, Avenue de la boulaie, 35576 Cesson Sévigné, France

Email: [jacques.weiss@centralesupelec.fr](mailto:jacques.weiss@centralesupelec.fr)

**Abstract**—This paper develops a new paradigm for the multi-input multi-output detection problem with bit interleaved coded modulation (MIMO-BICM). This new paradigm is based on a geometric method rather than the traditional interference cancellation or tree search. It describes in greater detail the soft-output detector called list exploration and exploitation (L2E), which builds a list of candidates from a geometrical interpretation of a given objective function. It then computes the log-likelihood ratios (LLRs) using the max-log approximation. A comparative study between L2E and a classical tree-based algorithm is carried out in both computational complexity and detection performance. This study highlights that although the framework is entirely different, the complexity and performance are comparable with the state of the art tree-based paradigm. Finally, the proposed algorithm is implemented on a field-programmable gate array (FPGA) device. Simulations carried out with Xilinx Vivado tools and measurements are provided to analyze the resource utilization, power consumption, and timing metrics. We further estimate these metrics for an application-specific integrated circuit (ASIC) implementation based on multiplicative factors from literature. This projection demonstrates that our implementation yields results of the same magnitude as the well-known detectors.

**Keywords**—Geometrical algorithm; MIMO detection; Complexity analysis; BER performance; FPGA; Max-log approximation

## I. INTRODUCTION

This paper carries on the work initiated in [1], where we described the interest of geometric detectors. It takes place in the context of MIMO systems that have been integrated into many standards, such as IEEE 802.11n [2] or long-term evolution (LTE). It is well known that increasing the number of antennas improves the data rate and the link reliability [3], but at the same time increases the complexity of detection at the receiver side. Detection problems can be classified into three types: over-determined MIMO, iso-determined MIMO, and under-determined MIMO.

Over-determined problems occur in particular in the massive MIMO uplink case, where a base station is equipped with a very large number of receiving antennas to detect messages from a small number of users. Under the hypothesis of a perfectly-known channel, the problem is very easily solved with linear detectors such as zero-forcing (ZF) or minimum

mean square error (MMSE). Linear detectors require the inversion of the channel matrix, which is the most complex step. Current research offers binary error rate (BER) efficient detectors with even less algorithmic complexity. These detectors approximate the MMSE criteria or the channel matrix inversion by conjugate gradient least square [4], symmetric successive over relaxation [5], Neumann series expansion [6] or using the Jacobi method [7].

For iso-determined systems, linear detectors cannot provide acceptable BER performance because there is just enough information available to retrieve the transmitted signal. In this situation, the maximum likelihood (ML) detector offers an optimal result at the cost of very high complexity. This complexity prevents its use for real-time hardware implementations, which is why simpler sub-optimal detectors are required. The earliest proposals were based on iterative detection using successive suppression of interference between antennas [8]. They led to the successive interference cancellation (SIC) and ordered successive interference cancellation (OSIC) detectors [9], [10] that are used nowadays. Parallel interference cancellation (PIC) is another variant of this paradigm [11], [12]. Subsequently, detectors based on tree-search became the reference with three variations: the breadth-first tree-search [13]–[16], the depth-first tree-search as the sphere decoding (SD) [17], [18] and the best-first or metric-first [19]. More exotic approaches have also been proposed, such as geometric detection [20], deep neural network detection [21] or bio-inspired algorithms [22].

Soft-output detectors are known to be more efficient than hard-output ones [23] because they exploit the uncertainty that a '0' or a '1' is being received to provide an LLR on the received bits. This probability is then used in conjunction with an error-correcting code to improve BER performance. Finding exactly the a-posteriori probabilities is known to be exponentially complex with respect to the number of transmitting antennas [24]. That is why the reference algorithms approximate the LLRs using the max-log approximation [23], [25], [26]. Thus, the large majority of soft-output MIMO detectors construct a list of possible candidates and then use this approximation to produce approached values of LLRs. Examples include the list sphere decoding [23] or the soft version of the breadth-first M-algorithm [13], [15].

In the last years, efforts have been made to propose very large scale integration (VLSI) implementations aiming for high throughput, low energy consumption, and high flexibility. Different architectures have been explored: arrays of reconfigurable units [5], [27]; pipelines with parallel units [16], [28]; systolic arrays [6] and multiple cores managed by a task scheduler [18].

In this paper, we detail more precisely the L2E algorithm [1], which builds a list from geometric considerations rather than from tree paths. In particular, we present some algorithmic improvements and compare the complexity to the one of tree-based detectors (i.e., detectors with quasi-optimal performance). We also present initial investigations on the hardware implementability of geometric algorithms. To do so, we provide the architecture of the corresponding hard-output detector and highlight the intrinsic parallel structure of this algorithm. Finally, we present Monte-Carlo simulations to compare L2E performance with the best-known detectors.

In Section II, we present the mathematical system model. Then we describe the L2E and K-best Schnorr-Euchner (KSE) algorithms in Section III. Subsequently, Section IV compares the two algorithms and Section V presents an FPGA-based hardware implementation. Finally, Section VI concludes this paper.

## II. MATHEMATICAL MODEL

In this paper, bold lower cases (*resp.* capital letters) denote vectors (*resp.* matrices) and other characters refer to scalars. We call  $\mathbf{v}(i)$  the  $i^{\text{th}}$  coefficient of the vector  $\mathbf{v}$  and  $\mathbf{A}(i, j)$  the coefficient on the  $i^{\text{th}}$  row and the  $j^{\text{th}}$  column of  $\mathbf{A}$ . In this section, we present the modeling of the MIMO-BICM system, detail the LLRs calculations and discuss on the advantages of the QR decomposition.

### A. MIMO-BICM system model

We consider a quadrature phase-shift keying (QPSK), and we note  $\phi$  the set of possible symbols. Let  $\mathbf{y}_c \in \mathbb{C}^M$  be the vector containing the signal received on the  $M$  reception antennas. These signals are the result of the  $N$  transmitted symbols  $\mathbf{x}_c \in \phi^N$  after passing through the channel described by the matrix  $\mathbf{H}_c \in \mathbb{C}^{M \times N}$  and after adding a Gaussian noise  $\mathbf{w}_c \in \mathbb{C}^M$ . With these notations, the transmission system is modeled by

$$\mathbf{y}_c = \mathbf{H}_c \mathbf{x}_c + \mathbf{w}_c. \quad (1)$$

For the sake of implementation, we propose a real-valued version of the previous model using  $\Re$  (*resp.*  $\Im$ ) the real (*resp.* imaginary) part operator. We introduce the real-valued equivalent of the previous vectors, matrix and set:

$$\mathbf{y} \triangleq \begin{bmatrix} \Re(\mathbf{y}_c) \\ \Im(\mathbf{y}_c) \end{bmatrix} \quad (2)$$

$$\mathbf{H} \triangleq \begin{bmatrix} \Re(\mathbf{H}_c) & -\Im(\mathbf{H}_c) \\ \Im(\mathbf{H}_c) & \Re(\mathbf{H}_c) \end{bmatrix} \quad (3)$$

$$\mathbf{x} \triangleq \begin{bmatrix} \Re(\mathbf{x}_c) \\ \Im(\mathbf{x}_c) \end{bmatrix} \quad (4)$$

$$\mathbf{w} \triangleq \begin{bmatrix} \Re(\mathbf{w}_c) \\ \Im(\mathbf{w}_c) \end{bmatrix} \quad (5)$$

$$\xi \triangleq \Re(\phi) \quad (6)$$

The MIMO-BICM model can now be expressed as

$$\mathbf{y} = \mathbf{H}\mathbf{x} + \mathbf{w}. \quad (7)$$

This real-model representation of (1) has exactly the same amount of information as the complex-valued version and we define  $n \triangleq 2N$ ,  $m \triangleq 2M$ . Indeed, it is like treating the real and imaginary axis independently. In the remainder, we assume  $n \leq m$ : we have at least as many receiving antennas as transmitting one.

This model can be used to describe any iso-determined or over-determined MIMO-BICM system. On transmission, the message is coded by an encoder, interleaved with an assumed perfect interleaver, and then mapped to symbols. On reception, the data flow is processed in the opposite way: it goes through a detector, a de-interleaver, and then a decoder. A perfect channel state information is assumed only at the reception, and no information at all is known at the transmitter.

### B. LLRs generation

Let us consider  $b_{ij}$  the  $i^{\text{th}}$  bit of information coded in the  $j^{\text{th}}$  component of  $\mathbf{x}$ . To minimize the BER, a soft detector must maximize the a posteriori probability that is calculated from the probability mass function  $P(b_{ij} | (\mathbf{H}, \mathbf{y}))$  of the bit  $b_{ij}$  given the state of the channel  $\mathbf{H}$  and the received vector  $\mathbf{y}$ . The LLR is defined as

$$L_{ij} = \ln \frac{P(b_{ij} = 1 | (\mathbf{H}, \mathbf{y}))}{P(b_{ij} = 0 | (\mathbf{H}, \mathbf{y}))}. \quad (8)$$

The closed-form evaluation is known to be exponentially complex with respect to the dimensions of the MIMO system [24]. This is why we use the classic max-log approximation [23], [25], [26]

$$L_{ij} \approx \frac{1}{2\sigma^2} \left( \min_{x \in \chi_{ij}^0} \|\mathbf{y} - \mathbf{H}\mathbf{x}\|_2^2 - \min_{x \in \chi_{ij}^1} \|\mathbf{y} - \mathbf{H}\mathbf{x}\|_2^2 \right) \quad (9)$$

where  $\chi_{ij}^k = \{x \in \xi^n : b_{ij} = k\}$  is the set of all symbols with  $b_{ij}$  equals to  $k$ , and  $\sigma^2$  is the noise variance. Although simpler, this new expression remains exponentially complex since we have  $\text{card}(\chi_{ij}^k) = 2^{n-1}$  where  $\text{card}()$  denotes the cardinality of a set. therefore, we introduce a new subset  $\Gamma \subset \xi^n$  representing a list of candidates and we compute LLRs only from this subset:

$$L_{ij} \approx \frac{1}{2\sigma^2} \left( \min_{x \in \Gamma \cap \chi_{ij}^0} \|\mathbf{y} - \mathbf{H}\mathbf{x}\|_2^2 - \min_{x \in \Gamma \cap \chi_{ij}^1} \|\mathbf{y} - \mathbf{H}\mathbf{x}\|_2^2 \right). \quad (10)$$

If  $\Gamma \cap \chi_{ij}^k = \emptyset$ , we consider that  $b_{ij}$  is different from  $k$  for sure and set  $L_{ij}$  to its maximum or minimum value in order to reflect this certainty.

The algorithmic cost to approximate LLRs is now fully controlled by  $\text{card}(\Gamma)$ : the more points in  $\Gamma$ , the better the approximation, but at the same time the more difficult the computation becomes. The L2E algorithm constructs a set  $\Gamma$  whose cardinal grows linearly with  $n$  and is independent with respect to the signal-to-noise ratio (SNR) values. In the remainder of this paper, we refer to  $\|\mathbf{y} - \mathbf{H}\mathbf{x}\|_2^2$  as the objective

function and the best points of a set refer to the points that minimize this  $\ell_2$ -norm.

### C. QR decomposition

QR decomposition is a well-known technique to simplify the norm evaluation. Let be  $\mathbf{H} = \mathbf{QR}$  the QR decomposition of the channel matrix with  $\mathbf{Q}$  an orthogonal matrix and  $\mathbf{R}$  an upper triangular matrix. Then we have:

$$\|\mathbf{y} - \mathbf{H}\mathbf{x}\|_2 = \|\mathbf{y} - \mathbf{QR}\mathbf{x}\|_2 = \|\mathbf{Q}^T\mathbf{y} - \mathbf{Q}^T\mathbf{QR}\mathbf{x}\|_2 \quad (11)$$

as orthogonal matrices act as isometries. Thus, by exploiting the property of orthogonal matrices  $\mathbf{Q}^T = \mathbf{Q}^{-1}$  this norm can be rewritten as

$$\|\mathbf{y} - \mathbf{H}\mathbf{x}\|_2 = \|\tilde{\mathbf{y}} - \mathbf{R}\mathbf{x}\|_2 \quad (12)$$

with  $\tilde{\mathbf{y}} \triangleq \mathbf{Q}^T\mathbf{y}$ .

We recognize the same pattern so that an algorithm able to solve the full matrix version can solve the QR-based version in a similar way. Because of this mathematical similarity, we will continue in the following to use the full-matrix notation. All the results obtained for the full-matrix version are directly applicable in the triangular case. Thus, unless otherwise stated, the following developments are valid in both cases, even if only the full-matrix case is described.

## III. ALGORITHMIC INTERPRETATION

In this section, we present an algorithm to obtain a set with a reduced cardinality without compromising decoding properties. The L2E detector is based on two steps: exploration and exploitation, which will be detailed in the first two subsections. Next, we will present a classical tree-based algorithm that will be used as a reference in the following.

### A. Exploration step

The exploration phase has two main objectives: to begin to create the  $\Gamma$  set for the LLRs' evaluations and to build a set of promising points  $\Gamma_b$  that will be processed by the exploitation step.

To achieve these objectives, we first rewrite the objective function by introducing the singular value decomposition (SVD) of  $\mathbf{H} = \mathbf{UDV}^T$  with  $\mathbf{U}$  and  $\mathbf{V}$  two orthogonal matrices and  $\mathbf{D}$  the diagonal matrix containing the singular values  $\{\lambda_i : 1 \leq i \leq n\}$ . The order of these values being arbitrary, we choose to number them in ascending order.

We introduce the starting point define by  $\mathbf{x}_0 = \mathbf{H}^{-L}\mathbf{y}$  where  $\mathbf{H}^{-L}$  denotes the left Moore-Penrose inverse of  $\mathbf{H}$ . Consequently, the objective function can be rewritten as

$$\|\mathbf{y} - \mathbf{H}\mathbf{x}\|_2^2 = (\mathbf{V}^T(\mathbf{x} - \mathbf{x}_0))^T \mathbf{D}\mathbf{U}^T\mathbf{U}\mathbf{D}(\mathbf{V}^T(\mathbf{x} - \mathbf{x}_0)). \quad (13)$$

As the vectors of  $\mathbf{V}$ , named  $\{\mathbf{v}_i : 1 \leq i \leq n\}$ , constitute a basis, we can define  $\{\alpha_i : 1 \leq i \leq n\}$  the coordinates of  $\mathbf{x} - \mathbf{x}_0$  on this basis. Using the orthogonality of  $\mathbf{U}$  and  $\mathbf{V}$  and the diagonality of  $\mathbf{D}$ , equation (13) leads to

$$\|\mathbf{y} - \mathbf{H}\mathbf{x}\|_2^2 = \sum_{i=1}^n \alpha_i^2 \lambda_i^2. \quad (14)$$

Let  $\Delta_i$  be the straight line passing through  $\mathbf{x}_0$  and directed by  $\mathbf{v}_i$ . One can note that (14) highlights that the objective function grows more slowly along the first  $\Delta_i$  rather than

along the last ones. Thus, promising points are more likely to be found around these first straight lines. Figure 1 illustrates the previous reasoning in the simplified case of a space of dimension  $n = m = 2$ . The black ellipses represent the evolution of the objective function along the two positions of  $\mathbf{x}$ . The objective function minimum is reached in  $\mathbf{x}_0$ . The two singular vectors  $\mathbf{v}_i$  and the corresponding lines  $\Delta_i$  are also plotted. We can see that the objective function grows more slowly along  $\Delta_1$  than along  $\Delta_2$ . In this example, the solution that minimize the objective function is the point  $\mathbf{x} = (-1, 1)$ . It is confirmed that this solution is located close to the line  $\Delta_1$ .

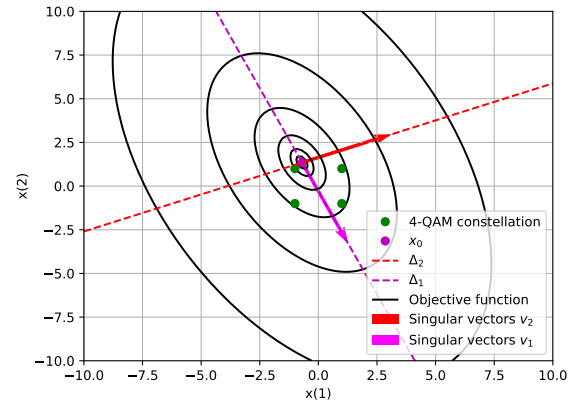


Figure 1. Link between the objective function and the SVD of  $\mathbf{H}$

There are several methods for choosing points near a line. To reduce the complexity, we choose to compute the intersection of the first straight lines with each hyperplane defined by  $\mathcal{H}_i = \{\mathbf{x} \in \mathbb{R}^n : \mathbf{x}(i) = 0\}$  and then to search in  $\xi^n$  for the nearest point to each intersections. Figure 2 illustrates, in the same situation as for Figure 1, the process of obtaining points from intersections. The points are obtained by a two-step process. First, the algorithm computes all the intersections between the line  $\Delta_1$  with the brown hyperplanes  $\mathcal{H}_i$ . Then, it searches for the nearest point in the constellation. When two points are equidistant, we take the closest to  $\mathbf{x}_0$ .

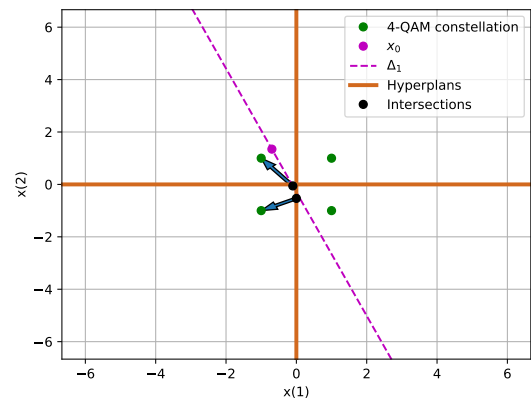


Figure 2. Getting promising points from a line  $\Delta_i$

The set  $\Gamma_b$  is obtained by picking the best  $C$  points obtained for each line  $\Delta$  considered. Thus, we have by construction  $\text{card}(\Gamma_b) = CD$ . Besides, all the points that have been computed are included to start building the set  $\Gamma$ . This operation does not cost anything since the points, and their objective function have already been calculated to obtain  $\Gamma_b$ . As better results are observed with  $x_0$  being the MMSE estimator, we use it in the following.

### B. Exploitation step

Exploitation step aims to enrich the already computed  $\Gamma$  set without increasing too much its size (i.e., the upper-bound of the number of added points is  $nCD$  per exploitation iteration). Let  $\mathcal{B}_{\mathbf{x},r}$  be the closed Hamming ball of radius  $r$  and centered at a point  $\mathbf{x}$ . To increase  $\text{card}(\Gamma)$ , we add each points in  $\mathcal{B}_{\mathbf{x},r}$  for all  $\mathbf{x} \in \Gamma_b$ . This process can be seen as flipping at most  $r$  bits of each procpoints in  $\Gamma_b$ . As there are  $\binom{n}{i}$  ways to change  $i$  bits among  $n$ , the exploitation of a point requires  $\sum_{i=0}^r \binom{n}{i}$  evaluations of the objective function. In order to reduce the computational complexity of the L2E detector, we fixed the value of  $r$  to 1. After one iteration, L2E makes a new one if it finds a better point in  $\mathcal{B}_{\mathbf{x},r}$  than the center of the ball (i.e., L2E iterates until it reaches a stable point).

After this second step, we obtain a set  $\Gamma$  such that

$$\text{card}(\Gamma) \leq (n_i + n)CD \quad (15)$$

where  $n_i$  is the number of exploitation iterations. This result is consistent with both the linear growth in the number of antennas and the independence from the SNR. Figure 3 gives an overview of the whole L2E algorithm where we recognize the pre-processing from instruction 1 to instruction 5, the exploration phase in the first for-loop, the exploitation phase in the last for-loop and eventually the soft-output computations to obtain LLRs at instruction 18. If the QR decomposition representation is adopted, its computation should be added in the pre-processing, and  $\tilde{\mathbf{y}}$  should be processed before the first for-loop.

### C. A tree-based reference: $K$ -best Schnorr-Euchner (KSE)

In this section, we will briefly describe a tree-based algorithm that will serve as a reference later on. We select the breadth-first algorithm KSE mode 1 without maximal radius as described in [14] since it is a well-known algorithm with a very acceptable complexity and performance. This algorithm also uses the max-log approximation and QR decomposition of the channel matrix and additionally requires that diagonal coefficients of  $\mathbf{R}$  to be in ascending order.

KSE first completes the QR decomposition transformation as described in Section II-C and then uses the triangularity of  $\mathbf{R}$  to compute the objective function iteratively. Thus, we can introduce  $\mathbf{d}(k) = \tilde{\mathbf{y}}(k) - (\mathbf{R}\mathbf{x})(k)$  such that the objective function is written as

$$\|\tilde{\mathbf{y}} - \mathbf{R}\mathbf{x}\|_2^2 = \sum_{k=1}^n \mathbf{d}(k)^2. \quad (16)$$

Moreover, triangularity gives for all  $k \in \{1, \dots, n\}$

$$(\mathbf{R}\mathbf{x})(k) = \sum_{j=1}^n \mathbf{R}(k,j)\mathbf{x}(j) = \sum_{j=k}^n \mathbf{R}(k,j)\mathbf{x}(j) \quad (17)$$

```

1 Extract the first  $D$  right singular vectors  $\mathbf{v}_i$  from  $\mathbf{H}$ 
2 Compute left pseudo-inverse  $\mathbf{H}^{-L}$ 
3 while  $\mathbf{H}$  does not change do
4   Compute starting point  $\mathbf{x}_0$ 
5   Initialize  $\Gamma$  with the projection of  $\mathbf{x}_0$  on  $\xi^n$ 
6   foreach  $\Delta$  in  $\{\Delta_1, \dots, \Delta_D\}$  do
7     foreach  $\mathcal{H}$  in  $\{\mathcal{H}_1, \dots, \mathcal{H}_n\}$  do
8       Find the intersection of  $\Delta$  with  $\mathcal{H}$ 
9       Project the intersection on  $\xi^n$ 
10      Evaluate objective function
11      Add the point to  $\Gamma$  and save its cost
12    Add  $C$  best points to  $\Gamma_b$ 
13  foreach  $\mathbf{x}$  in  $\Gamma_b$  do
14    Add the points in  $\mathcal{B}_{\mathbf{x},1}$  to  $\Gamma$ 
15    if there is a better point in  $\mathcal{B}_{\mathbf{x},1}$  than  $\mathbf{x}$  then
16      Center a new ball at this best point
17      Make a new iteration starting at line 13
18  Compute LLRs using (10)
19  return LLRs

```

Figure 3. L2E algorithm

that leads to

$$\mathbf{d}(k) = \tilde{\mathbf{y}}(k) - \sum_{j=k}^n \mathbf{R}(k,j)\mathbf{x}(j). \quad (18)$$

The basic idea underlying the KSE algorithm is to compute partial estimations of the objective function and  $\mathbf{d}(k)$  coefficients as the solution vector is built. Indeed, starting from the last component, it is possible to add a new operand in (16) as soon as a hypothesis is made on  $\mathbf{x}(j)$  since (18) is fully evaluated for this position. Figure 4 gives a brief overview of the KSE decoding process with  $\mathcal{X}$  being the set of partially constructed solutions. For the sake of readability, the indexes of the  $\mathbf{d}(k)$  and the objective function relating to each partially constructed vector are omitted, but there is one vector  $\mathbf{d}$  and one partial norm per solution in  $\mathcal{X}$ .

## IV. COMPARING THE TWO STRATEGIES

In this section, we provide a full analysis of the above algorithms in terms of hardware complexity (number of products and number of additions) and BER performance.

### A. Computational complexity

The complexity analysis should be done distinguishing between the pre-processing, which is performed once per coherence block and the decoding itself. Indeed, during a coherence block, several hundred symbol vectors can be sent [29]. That is why pre-processing does not profoundly impact the total complexity.

Concerning pre-processing, KSE requires a QR decomposition when L2E requires an SVD and the computation of a Moore-Penrose inverse. These two decompositions are known to have a cubic complexity in the largest size of the channel matrix [30]. It is noteworthy that the Moore-Penrose inverse can be obtained far more quickly based on an SVD of the

```

1 Compute QR-decomposition  $\mathbf{QR} = \mathbf{H}$ 
2 while  $\mathbf{H}$  does not change do
3   Compute  $\tilde{\mathbf{y}} = \mathbf{Q}^T \mathbf{y}$ 
4   Initialize the partial objective function at 0
5   Initialize  $\mathbf{d} = \tilde{\mathbf{y}}$ 
6   for  $k = n$  to 1 do
7     foreach  $x$  in  $\mathcal{X}$  do
8       foreach  $s$  in  $\xi$  do
9         Evaluate  $s\mathbf{R}(k, k)$ 
10        Update the partial  $\mathbf{d}(k)$ 
11        Update the partial objective function
12      Update  $\mathcal{X}$  by keeping the best  $K$  partial vectors
13      Update  $\mathbf{d}(j)$  for  $j \in \{1, \dots, k-1\}$ 
14  Compute LLRs using (18)
15  return LLRs

```

Figure 4. KSE algorithm

matrix. Thus, the pre-processing of L2E is faster than if the decomposition and inversion were performed independently. Finally, it should also be noted that a QR decomposition may be added to this pre-processing if this approach is adopted. To sum up, KSE has a slightly lighter pre-processing than L2E, but both have complexity in  $\mathcal{O}(m^3)$  products.

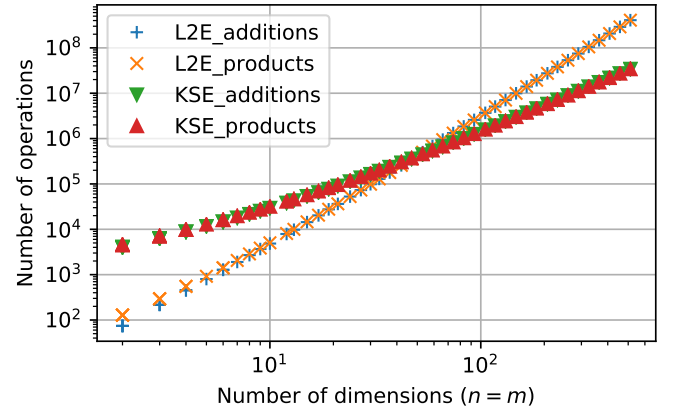
Table I details the complexity of each step of the L2E decoder for a QPSK depending on the parameters  $C$  and  $D$  and using the tricks presented in Section V-B. The addition of the calculation of  $\tilde{\mathbf{y}}$  in the QR-based setup would, in practice, reduce the number of operations required due to the triangularity of the channel matrix that speeds up the objective function evaluation. The experimental results presented in Section V-D2 support this point. As a comparison, we also evaluate KSE using a QPSK denoting by  $K$  the maximum number of paths kept at each step. KSE required  $4K$  additions and  $4K$  products per position to compute  $\mathbf{d}(k)$  and to update the partial objective function. Moreover, it also required some operations to update  $\mathbf{d}(k)$ , the amount depending on the processed coordinate. Indeed, (18) highlights that the fewer coordinates are left to process, and the fewer calculations are required.

TABLE I. Complexity of L2E assuming one exploitation iteration and KSE

Step	Additions	Multiplications
Compute $\mathbf{x}_0$	$nm$	$nm$
Intersections & Projections	$Dn^2$	$Dn^2$
Evaluate objective function	$Dn^2(m+1)$	$Dn^2m$
Exploitation step	$CDn(m+n+1)$	$CDn(m+n)$
Compute LLRs	1	0
<b>Asymptotic complexity L2E</b>	$\mathcal{O}(Dn^2m)$	$\mathcal{O}(Dn^2m)$

In total, the KSE algorithm has a lighter asymptotic complexity in  $\mathcal{O}(n(m+nK/2))$ . However, the number of antennas in a MIMO system is not always large enough to match the asymptotic behavior. For this reason, Figure 5 shows the exact number of operations depending on the number of antennas of a square MIMO ( $n = m$ ). We compare the two detectors on both the number of additions and products. These two numbers

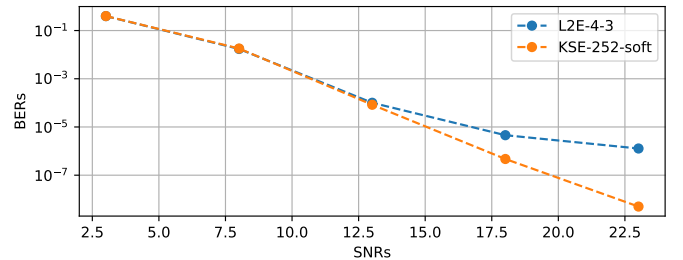
are very close, given that the most significant operation is the norm computations. One can note that both algorithms have an effective operating range with a cross-point around 16 antennas.

Figure 5. Number of operation of L2E ( $C = 4$ ,  $D = 3$ ) with soft KSE mode 1 ( $K = 252$ ) from [14] using a QPSK.

## B. BER performance

In this section, we propose Monte-Carlo simulations to evaluate the BER for different SNR =  $nE_s/N_0$  with  $E_s$  the average energy symbol and  $N_0$  the noise variance per entry [4]. We consider a MIMO-BICM system as modeled in Section II-A transmitting over an uncorrelated Rayleigh fading channel. The associate matrix  $\mathbf{H}$  is constructed as independent and identically distributed (i.i.d.) variables following a circularly-symmetric normal distribution and then transformed to its real-valued equivalent. Similarly,  $\mathbf{w}$  is elaborated with i.i.d. zero mean Gaussian noise with a variable variance to match the required SNR.

We assume a perfect interleaver so that all transmitted symbols are independent of one another. The binary data are mapped to a QPSK and encoded using a simple convolutional code of rate 1/2 generated by the polynomials (5, 7). The decoder uses the Viterbi algorithm with a traceback depth of 10. Figure 6 compares the performance of L2E using 3 singular directions and 4 candidates per directions ( $C = 4$  and  $D = 3$ ) with KSE using 252 paths in the case of a 4x4 MIMO ( $n = m = 8$ ). One can note that the performance is strictly equivalent up to 13 dB and that L2E loses only 2 dB for a BER of  $10^{-5}$  while requiring roughly six times fewer operations.

Figure 6. Performance comparison of L2E ( $C = 4$ ,  $D = 3$ ) with soft KSE mode 1 ( $K = 252$ ) from [14] on a 4x4 MIMO channel using a QPSK.

## V. FPGA IMPLEMENTATION

In this section, we present an exploratory work on the implementation of geometrical algorithms on FPGA hardware platforms. Given the exploratory nature of this work, we focus our description and implementation efforts on the most specific part of the L2E detector. The hardware platform selected is the Xilinx Zynq-7000 SoC that contains a 28nm programmable logic (PL) and an ARM processing system (PS). We choose to study only the hard algorithm [20] since it involves all steps but the LLRs computation. Moving from the hard version to the soft version only requires having a minimum search and a subtraction since all the norms required to calculate (10) are already provided by the hard part of the algorithm. This part is implemented using the PL.

The calculations that are well documented in the literature are performed upstream by the PS: SVD and QR decompositions and the  $\mathbf{x}_0$  calculation. The hardware architecture in PL described includes all the other stages, namely exploration and exploitation. Since this is an exploratory work, we have chosen to place parameterization and reusability before the performance, which is why we present an implementation using a data-driven pipeline where each module is independent of the others.

In the sequel, we set the  $n$ -dimension and the  $m$ -dimension to 10. We denote a fixed point quantization using the following notation: total word length is  $i + f$ , where  $i$  is the number of integer bits,  $f$  is the number of fractional bits. We summarize the fixed point design parameters for the reference solution  $\mathbf{x}_0$ , the directing vectors  $\{\mathbf{v}_i\}_{i=1}^D$ , the received vector  $\mathbf{y}$  and the entries of channel matrix  $\mathbf{R}$  in Table II.

TABLE II. Quantization of the fixed point parameters.

	Integer length	Fractional length	Total length
$\mathbf{x}_0$	3 bits	3 bits	6 bits
$\{\mathbf{v}_i\}_{i=1}^D$	1 bit	5 bits	6 bits
$\mathbf{y}$	6 bits	2 bits	8 bits
$\mathbf{R}$	6 bits	2 bits	8 bits

In this section, we will present the chosen FPGA architecture and detail the content of each module as well as the global structure based on a data-driven pipeline. Then, we give the results and compare them with the simulation and the current state-of-the-art literature. It is not straightforward to compare these results from a small FPGA with those from optimized ASICs. Some studies evaluated the performance gap between FPGAs and ASICs on general-purpose projects [31] and for convolutional neural networks (CNN) [32]. It is noteworthy that even if MIMO detection and CNN are two different problems, they are both mainly based on sum-product operations. These two studies draw similar factors on the performance gap on three quantities: clock frequency (which is comparable to throughput, resource use, and dynamic power consumption. Moreover, it is a common practice to scale up ASICs performance to 65nm CMOS. Table III details the mapping factors to be used to convert the results from a 28nm FPGA to a 28nm ASIC based on the performance gap highlighted earlier and then to a 65nm ASIC based on the same method as [16].

### A. FPGA architecture

Figure 7 shows the architecture considered as a simplified data flow and as a layout on the PL after the place and route

TABLE III. Multiplicative factor to approximate ASICs results

	28nm FPGA	28nm ASIC	65nm ASIC
Throughput ( $\sim f_{clk}$ )	1	3 to 6	1.3 to 2.6
Resource use / Area	1	1/30 to 1/13	1/5.6 to 1/2.4
Dynamic power consumption	1	1/14 to 1/12	1/6 to 1/5

optimizations. On the layout, we notice that the exploration modules noted D-1 and D-2 (for *diversification*) represent the most significant part of the area used. The four exploitation modules marked I (for *intensification*) are the second most important module in the resource use. The other slices relate to the interfaces and the final sorting.

The data flow diagram (Figure 7a) highlights the previously underlined parallelization, which is carried out at three levels. The  $D$  explorations are performed at the same time as the  $CD$  exploitations. Within these modules, the sub-modules are also executed in parallel: see, for example, the intersections and the computation of their norm. Finally, the internal operations within each sub-module can be parallelized using classical methods. It is evident, for example, that the contribution of each component of a vector can be treated independently when processing its norm. This data flow omits the data-driven synchronization modules for the sake of simplicity.

Two versions have been developed to check the decoding correctness and to measure the throughput. For the correctness verification, the PL is interfaced with the PS using AXI interfaces. The PS supplies the PL on request with the channel data ( $\mathbf{y}, \mathbf{H}$ ), the starting point  $\mathbf{x}_0$ , and the first singular vectors. The result is then returned to the PS that compares the solution to the one provided by the simulation. The throughput measurement is performed on PL without interaction with the PS to reduce its impact. The FPGA decodes 6365 datasets while counting the number of clock periods and then transmits this counter to the PL. The results of these tests are described in Section V-D.

### B. Module description

Exploration structure is straightforward as it is the direct transcription of the algorithm in Figure 3:  $\mathbf{x}_{ZF}$  and all  $\Delta \cap \mathcal{H}$  are processed and projected on  $\xi^n$ , the objective function (see (16)) is computed and then the  $C$  best points per direction are kept for the second step.

The exploitation module introduces the intermediate variable

$$\mathbf{\Omega} = \mathbf{y} - \mathbf{H}\mathbf{x} \quad (19)$$

to reduce the complexity of this step. Thus, once  $\mathbf{\Omega}$  is calculated, flipping the  $i^{\text{th}}$  components of  $\mathbf{x}$  only requires updating the preliminary result with

$$\mathbf{\Omega}_i = \mathbf{\Omega} - \mathbf{H}\mathbf{z} \quad (20)$$

where all the components of  $\mathbf{z}$  but the  $i^{\text{th}}$  are null. In addition, as we use a QPSK, the non-zero component is  $\mathbf{z}_i = -2\mathbf{x}_i$  and the update of the result can be reduced to  $n$  additions.

The two selection modules cannot use the same principle since one seeks a minimum norm while the other searches for several ones. The selection of the best point is made using a reduction tree in which each level contains a flip-flop. In contrast, the selection of the best  $C$  points is based on  $C$  registers containing the best norms encountered so far. These

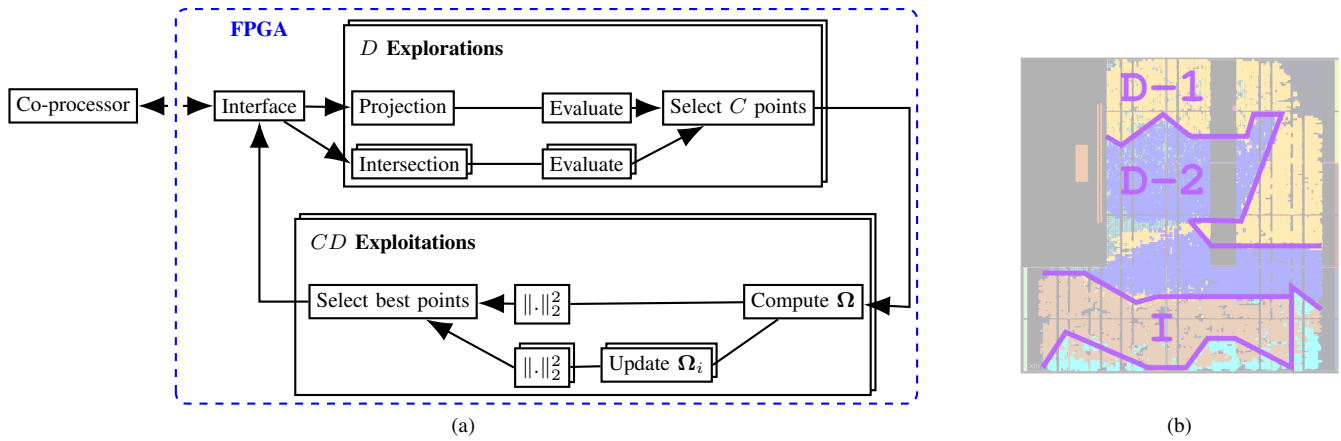


Figure 7. FPGA architecture implementing exploration and exploitation steps: (a) simplified data flow, (b) layout of main modules for  $C = D = 2$  where D-i refer to the  $i^{\text{th}}$  exploration module and I to the exploitation modules

registers are initialized with the highest possible norm. Then each candidate is inserted to maintain an increasing order among the registers. Thus, for each norm,  $C$  comparisons and at most  $C$  shifts are required. Table IV gives an example of the selection process.

TABLE IV. Example of selecting  $C = 3$  best points from 5 candidates

Input norm	Inserted in	Reg 0	Reg 1	Reg 2
26	Reg 0	max	max	max
15	Reg 0	26	max	max
25	Reg 1	15	26	max
19	Reg 1	15	25	26
34	Discarded	15	19	26
<b>Result</b>		<b>15</b>	<b>19</b>	<b>26</b>

### C. Data-driven pipeline

Data-driven pipeline is an approach adapted to prospective work since it divides the global system into small independent elements. Then, each sub-module can be developed and studied independently. This type of pipeline is close to the globally asynchronous locally synchronous (GALS) paradigm. Indeed, it requires an interface with a handshake protocol to control the data flow. Thus, each sub-module represented in Figure 7a is implemented as a GALS element, but the entire FPGA is clocked by the same signal, avoiding the potential metastabilities at the interfaces.

Regarding the interface, we use a single-rail 2-phase protocol as described in [33]: a request and acknowledgment signals are added to the data bus to control the propagation between the different stages. Each GALS interface is then equipped with a request port  $R$  driven by the sending module, an acknowledgment port  $A$  driven by the receiving module, and a data bus  $D$  driven by the sending one. Communications follow the given protocol with  $\bar{X}$  being the negation of  $X$  and  $\oplus$  the exclusive or:

- 1) Initially,  $R = A$  and the data bus state is unspecified.
- 2) When the sending module has some data to transmit, it sets  $D$  to the according value and sets  $R = \bar{A}$ . From this point, the data bus must keep its state.
- 3) The receiving module notices the event by testing  $R \oplus A$ , saves the data from  $D$ , and sets  $A = R$ . This module can start its computations.

- 4) The sending module takes note of the acknowledgment by processing  $R \oplus A$  and starts to process the next data, potentially changing the data bus state.

However, additional caution must be taken when there is more than one sender or receiver since there is no guarantee that the processing time is the same for all modules. Muller C-elements are therefore inserted on the  $A$  or  $R$  ports to transmit requests and acknowledgments only when all modules are ready. A Muller C-element is a gate that replicates the state of its inputs at its output if they are all identical and keeps its previous state otherwise [34].

### D. Result evaluation

As mentioned earlier, the evaluation of the results is done using two variants: one using the PL to check the decoding and one without to evaluate the throughput and resource use.

1) *Correctness test:* The correctness setup involves the PL and the PS and a computer that runs the equivalent decoding. The PS and the computer use a serial port to communicate. The computer starts by generating 500 datasets in the worst condition (SNR = 0dB) that contains a quantized version of a channel matrix, a received vector, the corresponding starting point, and two singular vectors. These values are then export as C files and fed to the PL by the PS. After decoding, the PS read the value from the PL and send it back to the computer through the serial port to be compared with the simulation results.

The PL decoding is compared with a double-valued simulation (i.e., the simulation with the best precision available used in Section IV-B) and a simulation with the same quantization as the hardware to check that it behaves as expected. Figure 8 represents the relative error on the final objective function as a histogram after 500 tests.

The right figure corresponding to the quantized simulation shows that the FPGA produces a solution with the same objective function as the simulation in the vast majority of tests and that the error is always lower than 15%. A closer look during the execution reveals that the errors are due to tricky situations where two choices are equivalent because of the quantization at one stage but do not produce an equivalent final solution. For example, two intersections with identical objective functions

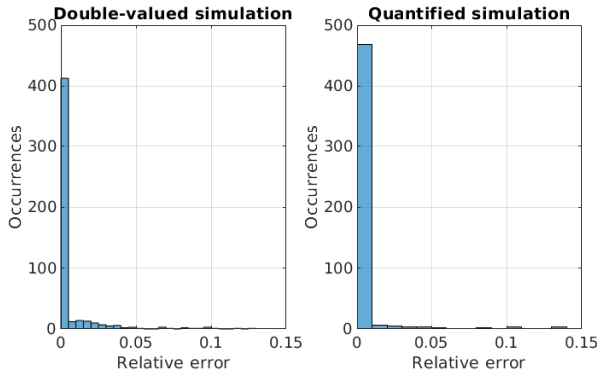


Figure 8. Histogram of the relative error between the simulation and the FPGA implementation over 500 tests

can be selected but do not give the same final point after the exploitation process. The left figure compares the hardware implementation with the perfect unquantized simulation. It indicates that quantization is not too damaging and validates the proof of concept, but a real system would require a better accuracy to obtain a valid BER.

2) *Throughput and resource use test*: The second test is performed without interacting with the PL to investigate the decoder without interference. Measurements are carried out after synthesis, placement, and routing in Vivado using the default settings. Results for the full channel matrix and the QR decomposition setup are compared on Table V when using the same frequency.

TABLE V. Implementation metrics (full matrix & QR-based matrix)

Channel matrix	Full	QR-based	Change
Clock frequency (MHz)	140	140	0
Look Up Tables (LUT) used	38 758	29 811	- 23 %
Flip-Flops (FF) used	40 708	37 630	- 7.56 %
Digital Signal Processors (DSP) used	110	70	- 36.4 %
Throughput (Mb/s)	7,88	26,9	+ 241 %
Dynamic power consumption (mW)	955	642	- 32.8 %

The first observation to be drawn from these results is that the QR decomposition greatly reduces the use of resources while increasing the throughput recorded. This is due to the reduction by a factor of almost two in the number of channel matrix coefficients that represent the largest part of the data. For example, in the case of  $n = m = 10$ , storing the full matrix requires  $n^2 = 100$  coefficients, however, the QR-based requires to store only  $\frac{n(n+1)}{2} = 55$  coefficients. For the rest of the processing, memory usage is shallow. Hence, the channel matrix entries storage has the most significant impact on block memory usage. Thus, by reducing the number of coefficients, we can significantly decrease the number of slices used to store the matrix in the pipeline and reduce the complexity during the placement and routing phase. Besides, the triangularity exploitation reduces the number of computations required for the norms evaluation, which represents the most complex step, as pointed out in Table I.

As stated earlier, it is unclear how these results can be compared with state of the art ASICs optimized implementations with whom the throughput spans from a dozen Mb/s to a few Gb/s [16]. However, we can get an insight into

the ASICs results based on the prediction factor described in Table III. Thus, we measured the throughput, and the dynamic power consumption of our 28nm FPGA implementation then multiplied by the projection factor to get the estimation of Table VI. One can notes that the proposed implementation would be in the lower range but would not be far behind. Moreover, we believe that switching from a data-driven pipeline to a fully synchronous implementation would significantly increase the performance leading to an even better result.

TABLE VI. Estimated performance on 65nm ASIC

	Actual 28nm FPGA	Prediction for 65nm ASIC
Throughput (Mb/s)	26.9	35 to 70
Dynamic power (mW)	642	107 to 129

## VI. CONCLUSION

In contrast to the main-stream detection paradigm, which is based on tree-search algorithms, this paper study a new paradigm, namely the geometrical algorithm. This paper highlights that geometrical detection can produce soft outputs using a list and the well-known max-log approximation. After describing the algorithm, we compared the complexity as well as the BER performance of these two approaches. We show that L2E is equivalent or only slightly inferior to the common KSE. Moreover, an implementability study is carried out on a Xilinx Zynq-7000 SoC using a data-driven pipeline. The results are validated by comparison to the simulation, and the resource use and the throughput are evaluated. This throughput is in the lower bound of the state-of-the-art, but it is important to note that references work on ASICs while we use an FPGA.

In light of these results, we think that even if the geometrical paradigm currently shows slightly inferior results that the tree-based one, it could lead to very efficient detectors in the future. Indeed, the tree-based paradigm is matured and has been developed for years, while geometrical detectors are instead on their beginning, and many improvements are still possible. For instance, we highlight that the hardware implementation throughput can be significantly increased by upgrading from FPGA to ASIC and from a data-driven pipeline to synchronous design. In the same way, BER performance could be easily improved by using an iterative detector-decoder framework as already done by the tree-based algorithms.

## REFERENCES

- [1] B. Trotobas and A. Nafkha, "Fixed Complexity Soft-Output Detection Algorithm Through Exploration and Exploitation Processes," in AICT 2018, Barcelona, Spain, Jul. 2018, pp. 89–93.
- [2] T. Paul and T. Ogunfunmi, "Evolution, insights and challenges of the PHY layer for the emerging IEEE 802.11n amendment," IEEE Communications Surveys & Tutorials, vol. 11, no. 4, 2009, pp. 131–150.
- [3] F. Rusek, D. Persson, B. K. Lau, E. G. Larsson, T. L. Marzetta, O. Edfors, and F. Tufvesson, "Scaling Up MIMO: Opportunities and Challenges with Very Large Arrays," IEEE Signal Processing Magazine, vol. 30, no. 1, Jan. 2013, pp. 40–60.
- [4] B. Yin, M. Wu, J. R. Cavallaro, and C. Studer, "Conjugate Gradient-based Soft-Output Detection and Precoding in Massive MIMO Systems," 2014 IEEE Global Communications Conference, Dec. 2014, pp. 3696–3701, arXiv: 1404.0424.
- [5] Q. Wei, L. Liu, G. Peng, S. Yin, and S. Wei, "Efficient and Flexible VLSI Architecture for Soft-Output Massive MIMO Detector," in Proceedings of Information Science and Cloud Computing. Guangzhou, China: Sissa Medialab, Feb. 2018, p. 055.

- [6] M. Wu, B. Yin, G. Wang, C. Dick, J. R. Cavallaro, and C. Studer, "Large-Scale MIMO Detection for 3gpp LTE: Algorithms and FPGA Implementations," *IEEE Journal of Selected Topics in Signal Processing*, vol. 8, no. 5, Oct. 2014, pp. 916–929, arXiv: 1403.5711.
- [7] X. Qin, Z. Yan, and G. He, "A Near-Optimal Detection Scheme Based on Joint Steepest Descent and Jacobi Method for Uplink Massive MIMO Systems," *IEEE Communications Letters*, vol. 20, no. 2, Feb. 2016, pp. 276–279.
- [8] P. W. Wolniansky, G. J. Foschini, G. D. Golden, and R. A. Valenzuela, "V-BLAST: an architecture for realizing very high data rates over the rich-scattering wireless channel," in *1998 URSI International Symposium on Signals, Systems, and Electronics. Conference Proceedings (Cat. No.98EX167)*, Oct. 1998, pp. 295–300.
- [9] A. Riadi, M. Boulouird, and M. M. Hassani, "ZF/MMSE and OSIC Detectors for UpLink OFDM Massive MIMO systems," in *2019 IEEE Jordan International Joint Conference on Electrical Engineering and Information Technology (JEEIT)*, Apr. 2019, pp. 767–772.
- [10] Hongyuan Zhang, Huaiyu Dai, and B. Hughes, "Analysis on the diversity-multiplexing tradeoff for ordered MIMO SIC receivers," *IEEE Transactions on Communications*, vol. 57, no. 1, Jan. 2009, pp. 125–133.
- [11] W. Chin, A. Constantinides, and D. Ward, "Parallel multistage detection for multiple antenna wireless systems," *Electronics Letters*, vol. 38, no. 12, 2002, p. 597.
- [12] C. Studer, S. Fateh, and D. Seethaler, "ASIC Implementation of Soft-Input Soft-Output MIMO Detection Using MMSE Parallel Interference Cancellation," *IEEE Journal of Solid-State Circuits*, vol. 46, no. 7, Jul. 2011, pp. 1754–1765.
- [13] K. K. Y. Wong and P. J. McLane, "A Low-Complexity Iterative MIMO Detection Scheme Using the Soft-Output M-Algorithm," *IST Mobile Summit*, Jun. 2005, p. 5.
- [14] Z. Guo and P. Nilsson, "Algorithm and implementation of the K-best sphere decoding for MIMO detection," *IEEE Journal on Selected Areas in Communications*, vol. 24, no. 3, Mar. 2006, pp. 491–503.
- [15] W. Shin, H. Kim, M. Son, and H. Park, "An Improved LLR Computation for QRM-MLD in Coded MIMO Systems," in *2007 IEEE 66th Vehicular Technology Conference*, Sep. 2007, pp. 447–451.
- [16] Z. Yan, G. He, Y. Ren, W. He, J. Jiang, and Z. Mao, "Design and Implementation of Flexible Dual-Mode Soft-Output MIMO Detector With Channel Preprocessing," *IEEE Transactions on Circuits and Systems I: Regular Papers*, vol. 62, no. 11, Nov. 2015, pp. 2706–2717.
- [17] U. Fincke and M. Pohst, "Improved methods for calculating vectors of short length in a lattice, including a complexity analysis," *Mathematics of Computation*, vol. 44, no. 170, 1985, pp. 463–471.
- [18] P. I.-J. Chuang, M. Sachdev, and V. C. Gaudet, "VLSI implementation of high-throughput, low-energy, configurable MIMO detector," in *2015 33rd IEEE International Conference on Computer Design (ICCD)*. New York City, NY, USA: IEEE, Oct. 2015, pp. 335–342.
- [19] G. He, X. Zhang, and Z. Liang, "Algorithm and Architecture of an Efficient MIMO Detector With Cross-Level Parallel Tree-Search," *IEEE Transactions on Very Large Scale Integration (VLSI) Systems*, 2019, pp. 1–13.
- [20] A. Nafkha, E. Boutillon, and C. Roland, "Quasi-maximum-likelihood detector based on geometrical diversification greedy intensification," *IEEE Transactions on Communications*, vol. 57, no. 4, Apr. 2009, pp. 926–929.
- [21] N. Samuel, T. Diskin, and A. Wiesel, "Deep MIMO detection," in *2017 IEEE 18th International Workshop on Signal Processing Advances in Wireless Communications (SPAWC)*, Jul. 2017, pp. 1–5, iSSN: 1948-3252.
- [22] A. Datta and V. Bhatia, "A near maximum likelihood performance modified firefly algorithm for large MIMO detection," *Swarm and Evolutionary Computation*, vol. 44, Feb. 2019, pp. 828–839.
- [23] B. Hochwald and S. ten Brink, "Achieving near-capacity on a multiple-antenna channel," *IEEE Transactions on Communications*, vol. 51, no. 3, Mar. 2003, pp. 389–399.
- [24] C. Xu, D. Liang, S. Sugiura, S. X. Ng, and L. Hanzo, "Reduced-Complexity Approx-Log-MAP and Max-Log-MAP Soft PSK/QAM Detection Algorithms," *IEEE Transactions on Communications*, vol. 61, no. 4, Apr. 2013, pp. 1415–1425.
- [25] W. Koch and A. Baier, "Optimum and sub-optimum detection of coded data disturbed by time-varying intersymbol interference (applicable to digital mobile radio receivers)," in *Proceedings GLOBECOM '90: IEEE Global Telecommunications Conference and Exhibition*, Dec. 1990, pp. 1679–1684.
- [26] P. Robertson, E. Villebrun, and P. Hoeher, "A comparison of optimal and sub-optimal MAP decoding algorithms operating in the log domain," in *Proceedings IEEE International Conference on Communications*, vol. 2, Jun. 1995, pp. 1009–1013.
- [27] B. Yin, M. Wu, J. R. Cavallaro, and C. Studer, "VLSI design of large-scale soft-output MIMO detection using conjugate gradients," in *2015 IEEE International Symposium on Circuits and Systems (ISCAS)*. Lisbon, Portugal: IEEE, May 2015, pp. 1498–1501.
- [28] M. S. Khairy, C.-A. Shen, A. M. Eltawil, and F. J. Kurdahi, "Algorithms and Architectures of Energy-Efficient Error-Resilient MIMO Detectors for Memory-Dominated Wireless Communication Systems," *IEEE Transactions on Circuits and Systems I: Regular Papers*, vol. 61, no. 7, Jul. 2014, pp. 2159–2171.
- [29] E. Bjrnson, E. G. Larsson, and T. L. Marzetta, "Massive MIMO: Ten Myths and One Critical Question," *IEEE Communications Magazine*, vol. 54, no. 2, Feb. 2016, pp. 114–123, arXiv: 1503.06854.
- [30] G. H. Golub and C. F. Van Loan, *Matrix computations*, 4th ed., ser. Johns Hopkins studies in mathematical sciences. Baltimore, Md: Johns Hopkins Univ. Press, 2013, oCLC: 824733531.
- [31] I. Kuon and J. Rose, "Measuring the Gap Between FPGAs and ASICs," *IEEE Transactions on Computer-Aided Design of Integrated Circuits and Systems*, vol. 26, no. 2, Feb. 2007, pp. 203–215.
- [32] A. Boutros, S. Yazdanshenas, and V. Betz, "You Cannot Improve What You Do not Measure: FPGA vs. ASIC Efficiency Gaps for Convolutional Neural Network Inference," *ACM Transactions on Reconfigurable Technology and Systems*, vol. 11, no. 3, Dec. 2018, pp. 1–23.
- [33] M. Krstic, E. Grass, and X. Fan, "Asynchronous and GALS Design -Overview and Perspectives," in *2017 New Generation of CAS (NG-CAS)*, Sep. 2017, pp. 85–88.
- [34] D. E. Muller, *University of Illinois at Urbana-Champaign. Graduate College. Digital Computer Laboratory, and University of Illinois at Urbana-Champaign. Department of Computer Science, Theory of asynchronous circuits.* Urbana, Illinois : University of Illinois, Graduate College, Digital Computer Laboratory, 1955.

## AI Based Beam Management for 5G (mmWave) at Wireless Edge

Chitwan Arora, Hughes Systique Corporation, Gurgaon, India,  
chitwan.arora@hsc.com

Abheek Saha, Hughes Systique Corporation, Gurgaon, India,  
abheek.saha@hsc.com

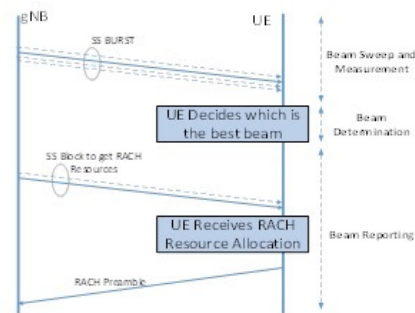
**Abstract**—Fast and accurate beam shaping mechanism is the key enabler in the use of millimeter-wave in the 5th Generation cellular systems in order to achieve low latency and high data rate requirements. Recent advances in Deep Learning (DL) has shown that Deep Learning (DL) based techniques can play a significant role in efficient beam shaping. For effective operation, it is essential that the ML based beam management algorithm should be deployed at the place in network where all the relevant input parameters needed for beam management are available continuously as well as the output of the beam management can be applied instantly. In this paper, we shall demonstrate how an edge-based Deep Learning program can be used to implement adaptive mm-wave beam-shaping, so as to optimally use millimeter wave channels.

**Keywords**—mmWave; beam shaping; machine learning; double directional channel ; wireless edge.

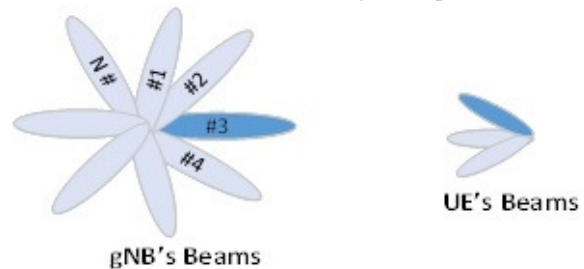
### I. INTRODUCTION

The millimeter wave (mmWave) frequencies offer the availability of huge bandwidths to provide unprecedented data rates demand for Fifth Generation (5G) applications. However, mmWave links are highly directional and are susceptible to severe free space pathloss and atmospheric absorption. To address these challenges, the base stations and the mobile terminals use directional antenna arrays and dynamic phase shifting to achieve sufficient link budget in wide area networks. Directional links, however, require fine alignment of the transmitter and receiver beams, achieved through a set of operations known as beam shaping. These operations are fundamental to the performance of a variety of control tasks . For example, one of these tasks is the Initial Access (IA) for idle-mode users, which allows a mobile User Equipment (UE) to initiate and establish a physical link connection with a gNB (5G base station). A second operation is Beam tracking, which enable beam adaptation schemes, or handover, path selection and radio link failure recovery procedures for connected millimeter wave user terminals [1,2].

In figure 1, we show a few steps in the beam management procedure for 5G Stand Alone (SA) scheme. In existing Long-Term Evolution (LTE) systems (using spectrum in 3-5 GHz), these control procedures are performed using omnidirectional signals, and beamforming or other directional transmissions can only be performed after a physical link is established, for data plane transmissions. However, in mm-wave access, due to the extreme directionality of the channels, it is essential to exploit the antenna gains even during initial access and for all control operations, even though they require a very small amount of data exchange.



(a) Standalone beam-management procedure



(b) Sequential Beam Sweeping

Fig. 1. Beam Management options in 5G networks

Hence, there is a need for precise alignment of the transmitter and the receiver beams while minimizing the time taken in beam acquisition and training. The initial access in 5G millimeter wave is a time-consuming search to determine suitable directions of transmission and reception. For example, in the cell discovery phase, one approach is sequential beam sweeping by the base station that requires a brute force search through many beam-pair combinations between UE and gNB to find the optimum beam-pair i.e., the one with the highest reference received signal power (RSRP) level, as shown in Figure 1b. The sequential search may result in a large access delay and low initial access efficiency. It also consumes a fair amount of energy in the receiver, which makes it unsuitable for energy constrained receivers, such as Internet of Things (IoT) endpoints.

Even if we use the existing LTE techniques of having a wide area beam for initial attachment and then data connection on the mm-wave beams, the beam shaping problem is only deferred to the PDSCH selection phase. Additionally, the PDSCH requires far better alignment than the PDCCH, because of the higher data rates required.

In existing LTE systems, DL channel quality is estimated from an omnidirectional signal called the Cell Reference Sig-

nal (CRS) [3] for beam alignment and selection in connected state. CRS is regularly monitored by each UE in connected state to create a wideband channel estimate that can be used both for demodulating downlink transmissions and for estimating the channel quality [4]. In 5G mmWave networks CRS-based estimation is challenging due to the directional nature of the communication, thus requiring the network and the UE to constantly monitor the direction of transmission of each potential link. Tracking changing directions can decrease the rate at which the network can adapt and can be a major obstacle in providing robust and ubiquitous service in the face of variable link quality. In addition, UE and gNB may only be able to listen to one direction at a time, thus making it hard to receive the control signaling necessary to switch paths. Recent studies by [5] and others establish that the typical millimeter wave channel has multiple rays, but each ray has a very narrow boresight, hence offering very small degrees of error tolerance. From the above description, it is apparent 5G networks should support a mechanism by which the users and the infrastructure can quickly determine the best directions to establish the mmWave links. These are particularly important issues in 5G networks and motivate the need to extend current LTE control procedures with innovative mmWave-aware beam management algorithms and methods. In this paper, we have proposed a Deep Learning based algorithm for predicting channel parameters based on user location. Combined with a simple offset based precoder, we have shown how our Deep Learning algorithm allows us to acquire optimal channels relatively quickly as compared to conventional search based techniques. We have justified this, using simulation results using real-life data from a ray-tracing model developed by [30]. It has been observed that the online DL based techniques gives superior performance than offline DL based techniques. Online DL techniques efficiently adapt themselves to support high mobility in mmWave systems. Deployment strategy for the training of these deep learning algorithm has been explored in this paper. and it has been proposed that wireless edge is the appropriate place for the deployment of these DL based algorithm for beam management. Since our proposed algorithm runs in realtime, we shall show that is suitable for deployment in a hybrid form, with the training being done in the cloud and the actual prediction taking place in the wireless edge. The remainder of this paper is organized as follows. Section II discusses the literature survey of traditional (non- ML/DL) as well as ML/DL based beam management techniques which have been proposed in recent years. In Section III we introduce the formal model of the mm-wave channel and propose a simple offset based algorithm which can be used for beam-shaping, once the channel parameters have been estimated. In Section IV we discuss the design of the deep learning algorithm, the data set used for training and testing the associated challenges of implementation. Finally, in Section V we provide our simulation results, discuss the deployment considerations at the edge and finish with our the conclusions.

## II. LITERATURE SURVEY

In the following section, work related to traditional (Non-ML/DL) and ML/DL based beam management has been captured.

### A. Traditional (Non-ML/DL) based beam management

Several approaches for directional based schemes has been proposed in the literature, to enable efficient control procedures for both the idle and the connected mobile terminals. Most literature on Initial Access and tracking refers to challenges that have been analyzed in the past at lower frequencies in ad hoc wireless network scenarios or, more recently, referred to the 60 GHz IEEE 802.11ad WLAN and WPAN scenarios (e.g., [6,7,8]). However, most of the proposed solutions are unsuitable for next-generation cellular network requirements and present many limitations (e.g., they are appropriate for short range, static and indoor scenarios, which do not match well the requirements of 5G systems). In [9,10], the authors propose an exhaustive method that performs directional communication over mmWave frequencies by periodically transmitting synchronization signals to scan the angular space. The result of this approach is that the growth of the number of antenna elements at either the transmitter or the receiver provides a large performance gain compared to the case of an omnidirectional antenna. However, this solution leads to a long duration of the Initial access with respect to LTE, and poorly reactive tracking.

Similarly, in [11], measurement reporting design options are compared, considering different scanning and signaling procedures, to evaluate access delay and system overhead. The channel structure and multiple access issues are also considered. The analysis demonstrates significant benefits of low-resolution fully digital architectures in comparison to single stream analog beamforming. More sophisticated discovery techniques are reported in [12,13] to alleviate the exhaustive search delay through the implementation of a multi-phase hierarchical procedure based on the access signals being initially sent in few directions over wide beams, which are iteratively refined until the communication is sufficiently directional. In [14], a low-complexity beam selection method by low-cost analog beamforming is derived by exploiting a certain sparsity of mmWave channels. It is shown that beam selection can be carried out without explicit channel estimation, using the notion of compressive sensing. The issue of designing efficient beam management solutions for mmWave networks is addressed in [15], in which the author designs a mobility-aware user association strategy to overcome the limitations of the conventional power-based association schemes in a mobile 5G scenario.

Other relevant papers on this topic include [16], in which the authors propose smart beam tracking strategies for fast mmWave link establishment the algorithm proposed in [17] takes into account the spatial distribution of nodes to allocate the beam width of each antenna pattern in an adaptive fashion and satisfy the required link budget criterion. Since the proposed algorithm minimizes the collisions, it also minimizes the average time required to transmit a data packet from the

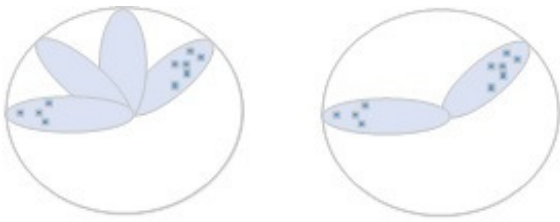


Fig. 2. Beam Sweeping in sparsely distributed UE Scenario

source to the destination through a specific direction. In 5G scenarios, some papers [9,10,11] give some insights on trade-offs among different beamforming architectures in terms of user communication quality. Finally, in [18,19], the authors evaluate the mmWave cellular network performance while accounting for the beam training, association overhead and beamforming architecture. The results show that, although employing wide beams, initial beam training with full pilot reuse is nearly as good as perfect beam alignment.

### B. ML/DL based beam management

The recent progress in Machine learning and Deep Learning has raised interest in applying these techniques to communication system related problem [20,21,22,23,24,25,26]. On the same lines compared to the traditional beam management approaches data-driven Deep learning-based approaches has been used for efficient beam management. The key idea is that ML/DL is used to make recommendations of promising beam pairs based on the various system parameters as well as past beam measurements. Within the mm-wave systems, ML/DL have been discussed for three specific functions. The first is beam-sweeping (Figure 2), which refers to the generic problem of determining how the coverage area is to be *swept* by the pilot beam(s), so as to optimize coverage and capacity. There are various papers which focus on predicting the proposed Beam sweeping pattern based on the dynamic distribution of user traffic. In [27], a form of recurrent neural networks (RNNs) called a Gated Recurrent Unit (GRU) has been proposed. In this paper, the spatial distribution of users is inferred from data in Call Detail Records (CDRs) of the cellular network. Results show that the spatial distribution of the user population and their approximate location (direction) can be accurately predicted based on CDRs data using GRU, which is then used to calculate the sweeping pattern in the angular domain during cell search. In [28] beam sweeping pattern based on Gated Recurrent Unit (GRU) is compared with random starting point sweeping to measure the synchronization delay distribution. Results shows that this deep learning beam sweeping pattern prediction enable the UE to initially assess the gNB in approximately 0.41 of a complete scanning cycle with probability 0.9 in a sparsely distributed UE scenario. In Figure 2 it has been demonstrated that in case of sparsely distributed UE scenario, DL based techniques can help to reduce the number of beams to be traversed during beam sweeping. As a result, it will reduce the sweeping time drastically.

A second area of usage is in fast-beam alignment (Figure 3) for which the position information may be leveraged.



Fig. 3. Beam Management based on Position Information

Inverse fingerprinting is one approach to exploit position information [29], which works in Non-Line-of Sight (NLOS) channels. There are multiple research papers [30,31,32] which focus on using machine learning to make recommendations of promising beam pairs based on the location of the UE position relative to the gNB and past beam measurements. The UE location and past beam measurements can be input into a learning algorithm that learns to rank promising beam directions. By prioritizing beam training in top-ranked directions, the training overhead can be reduced. Figure 3 shows the steps of beam management based on Position Information.

In [31], the author proposes UE position-based beam alignment in the context of vehicular communication. that this inverse fingerprinting method is efficient. However, the proposed approaches have some limitations. First, the approach is offline, which means its use is delayed until the database is collected. Second, also due to being offline, its performance depends entirely on the accuracy of the collected database, which may become stale over time. To overcome these shortcoming Online approaches have been proposed. In the online approach it has been proposed to keep collecting new observations during operation, making it possible to improve the database. Machine learning tools combined with awareness of the proximity situation has been proposed in [33] to learn the beam information (power, optimal beam index, etc.) from past observations. In this paper, situational awareness that are specific to the vehicular setting including the locations of the receiver and the surrounding vehicles has been considered. The result shows that situational awareness along with machine learning can largely improve the prediction accuracy and the model can achieve throughput with little performance loss with almost zero overhead.

Finally, we have coordinated beamforming, where multiple base-stations or radio-heads simultaneously try to optimize their beams so as to target a user or a population of users. A coordinated beamforming solution using deep learning was proposed in [34]. In this paper, the received training signals via omni-reception at a set of coordinating Base Stations (BSs) are used as the input to a deep learning model that predicts the beamforming vectors at those BSs to serve a single user. These coordinated beamforming deep learning techniques are based on supervised learning techniques, which assume an offline learning setting and require a separate training data collection phase. However, there are papers which focus on online learning algorithms using the Multi Armed Bandit (MAB) framework, which is a special class of Reinforcement Learning (RL). Further, the work in [32,35,36] propose beam alignment techniques using Machine Learning. Position-aided beam prediction was proposed in [32,35]. Decision tree learning was used in [35],

and a learning-to rank method was used in [32]. The work in [32,35,36] shows that machine learning is valuable for mmWave beam prediction.

### III. THE PROBLEM OF CHANNEL ESTIMATION

In order to implement any kind of beam-shaping, we must first understand the relevant channel characteristics. In this section, we consider the specifics of the mm-wave channel in more detail. On the basis of multiple empirical studies [5,37] the currently most widely accepted channel model for mm-wave systems is the clustering model proposed by ITU-T. Here, the signal is assumed to be received in  $K$  clusters; each cluster is modelled in terms of a power fraction, an angle of arrival/departure, the beamsread (which measures the dispersion of the AoA/AoD) and a delay spread. In [38], the authors make an empirical measurements based on this cluster model for the 28Ghz and 73Ghz channels. The data shows that a typical channel has  $1 \leq K \leq 4$  clusters, where the strongest cluster component contains approximately 60% of the total power. The horizontal angular spread was of the order of  $1^\circ$ . In other words, the clusters have highly specific beam directions, with relatively tight angular dispersion.

#### A. DFT based beam-shaping for directional channels

In this section, we introduce the a mathematical model of the multi-antenna transceiver for the mm-wave channel. We consider a linear array of receivers with inter-receiver spacing  $d$ , receiving a signal of wavelength  $\lambda$ . The receive signal has wavelength  $\lambda$ . The transmit signal has a spatial amplitude distribution given by  $s(\theta)$ ,  $-\pi/2 \leq \theta \leq \pi/2$ , where  $\theta$  is an angle of arrival (with respect to the normal of the antenna array) in the plane of the array. The corresponding intensity of the recieved signal as a function of any arbitrary direction  $\theta$  in (1) of (1).

$$\mathcal{G}(\theta) = s(\theta) \sum_{m=0}^{M-1} e^{jk\omega} w_k \quad (1)$$

$$\omega = 2\pi \frac{d}{\lambda} \sin(\theta) \quad (2)$$

$$I(\theta) = [s(\theta)\mathcal{G}(\theta)]^2 = s^2(\theta) \left( \frac{1 - e^{jM\omega}}{1 - e^{j\omega}} \right)^2 \quad (3)$$

Typically,  $d/\lambda$  is standardized to a fraction  $d_f$  which is usually set to 0.5 or 0.25, tuned for the particular spectrum we are interested in. The maximum intensity is at  $M\omega = -\pi/2 \Rightarrow \theta = \sin^{-1} \left( \frac{1}{2Md_f} \right)$ . In most cases, the transmit signal comes from a specific direction  $\theta_d$ , which means that the function  $s(\theta)$  can be represented as a Dirac delta function  $s(\theta) = \delta(\theta - \theta_d)$  or possibly a sharp pulse function like a root raised cosine function  $s(\theta) = \text{rrc}(\theta_d, \beta)$ . The receiver needs to ensure that the equation (3) has a maximum at  $\theta = \theta_d$ , so as to gather the signal from the optimal direction. In that case, we add a artificial phase shift  $\Psi = [1 \ e^\psi \ e^{2\psi} \ \dots \ e^{(M-1)\psi}]$  between successive

elements of the array. The equation (3) gets converted to (4), by introduction of the phase shift vector.

$$\begin{aligned} \omega &= \pi d_f \sin(\theta_d) + \psi = -\frac{\pi}{2M} \\ \psi &= -\frac{\pi}{2M} - \pi d_f \sin(\theta_d) \\ &\approx -\pi d_f \sin(\theta_d), M \rightarrow \infty \end{aligned} \quad (4)$$

The double-directional channel is a straightforward extension of this, except that each of the transmitter and the receiver have to independently choose their optimal phase shifts tuned to their specific directions. The mm-wave channel is a combination of  $L > 1$  double directional channels or paths, each path associated with a delay  $\tau_l$ , complex attenuation  $\beta_l$  and a specific pair of AoD/AoA angles  $\phi_{l,t}, \phi_{l,r}$ , where  $1 \leq l \leq L$ . As stated above, we need to *beamshape* the transmit/receive arrays independently so as to achieve the optimum directional tuning; because we have  $L$  paths and not just one, the optimization is a more challenging problem. To this end, we introduce the beamshaping vector in each direction as  $\mathcal{B}_t = [b_{1,t} \ b_{2,t/r} \ \dots \ B_{N,t}]$  and the equivalent for the receive side, where  $\|\mathcal{B}_t\| = 1$  to maintain the power transmission constraint. The transmit signal can now be written as in (5)

$$\mathcal{G}_t(\theta_t) = \sum_{k=1}^N b_{k,t} e^{j\omega_{t,k}} \quad (5)$$

#### B. Beamshaping by choosing an appropriate offset angle

In this section, we shall outline a simple beamshaping algorithm which can be implemented in real-time for a multiple-cluster channel, based on the beam-directions (angles of arrival and departure). It has much lower computation load than the traditional optimization algorithms and its performance improves as the number of transmit/receive antenna (the size of the MIMO) increases. We first define the function  $g(\theta) = \exp\{-j2\pi\theta\}$  and note that by our definition that  $g(\cdot)$  has the following properties.

$$\begin{aligned} g^*(\theta) &= g(-\theta) \\ g(\theta_1) \cdot g(\theta_2) &= g(\theta_1 + \theta_2) \\ g(\theta) \cdot g^*(\theta) &= 1 \end{aligned} \quad (6)$$

We then define the column vector  $\alpha_N(\theta)$  as in (7)

$$\alpha(\theta) = \begin{bmatrix} 1 \\ g(\theta) \\ g(2\theta) \\ \vdots \\ g((N-1)\theta) \end{bmatrix} \quad (7)$$

We note that the transmit channel  $\alpha(\theta_t)$  and the beamforming matrix  $\mathcal{M} = [\alpha(\theta_1) \ \alpha(\theta_2) \ \dots \ \alpha_N(\theta_M)]$  should be such that the vector product of the two has just one of the entries to be non-zero; in [39], the authors introduce a metric of dispersion which measures precisely this. We can achieve this if  $\mathcal{M}$  is orthonormal and  $\alpha(\theta)$  is aligned to one of the columns in  $\mathcal{M}$ . Orthonormality for  $\mathcal{M}$  is equivalent to the

condition  $\alpha(\theta_i)^H \cdot \alpha(\theta_j) = 0$  for  $i \neq j$ . From (7), we get the expression for the vector product as in (8)

$$\begin{aligned} \alpha(\theta_i)^H \alpha(\theta_j) &= \sum_{k=0}^{N-1} g(-k\theta_i)g(k\theta_j) \\ &= \sum_{k=0}^{N-1} g(k(-\theta_i + \theta_j)) \\ &= \frac{1 - g(N(-\theta_i + \theta_j))}{1 - g(-\theta_i + \theta_j)} \end{aligned} \quad (8)$$

$$= \frac{1 - e^{j2\pi(\theta_i - \theta_j) \cdot N}}{1 - e^{j2\pi(\theta_i - \theta_j)}} \quad (9)$$

Setting the last expression of (8) to 0, we get that the condition is effectively that  $\theta_i - \theta_j = l/N$  for any non-zero integer  $l$ . A suitable choice for  $\theta_i = \frac{k}{N} + \phi$ ,  $-N/2 + 1 \leq k \leq N/2$ . We note that this is equivalent to the product of the  $N$  point DFT matrix  $\mathcal{W}$  and a diagonal phase-rotation matrix  $\mathcal{D}_\phi = \text{diag} [g(\phi) \ g(\phi) \ \dots]$ .

We now consider a single ray defined by the 3-tuple  $\langle \beta, \theta_t, \theta_r \rangle$  corresponding to the fading, the angle of departure from the transmitter and the angle of arrival to the receiver respectively. The corresponding channel matrix is defined in terms of the matrix product  $H = \beta (\alpha(\theta_r)\alpha(\theta_t)^H)$ . We assume that the transmitter has  $P$  antennae and the receiver  $Q$  antennae.

We now show a simple technique by which to beam-shape the transmission, so that the virtual channel matrix  $H_v$  has minimum dispersion of channel energy. To implement this, we find, for each of the transmitter and receiver,  $0 \leq p, q \leq N - 1$ , so that  $p/P, q/Q$  are the closest to  $\theta_t, \theta_r$  amongst all possible values of  $p, q$ . We then choose phase angles  $\phi_r, \phi_t$  such that  $q/N + \phi_r = \theta_r$ ,  $p/N + \phi_t = \theta_t$ . If we then construct transmit and receive precoding matrices  $\mathcal{V}_t = \mathcal{W}_P \mathcal{D}_{\phi_t}$ ,  $\mathcal{V}_r = \mathcal{W}_Q \mathcal{D}_{\phi_r}$ , we can show that the resultant virtual channel matrix has non-zero entries only on the  $p$  and  $q$  diagonal entries. Because the phase angle shift is constant, the orthonormality of the DFT matrix is retained due to the nature of (9). We note that  $p$  does not necessarily have to be the smallest value; any value of  $p, q$  is adequate provided that  $|\theta_t - p/P| \leq 1/P$  and equivalently for  $\theta_r, q, Q$ .

1) *The effect of error:* We consider the scenario where the estimated transmit angle  $\hat{\theta}_t = \theta_t + \delta_t$ . The corresponding  $\hat{\psi}_t$  will also change; the change is not linear in the error term, because of the implicit modulus over  $1/P$ .

$$\begin{aligned} \alpha[\theta_t] \alpha^*[\theta_t + \delta_t] &= \sum_k g(k\theta_t) g^*(k\theta_t) \cdot g(k\delta_t) \\ &= \sum_k g(k\delta_t) = \frac{1 - g(P\delta_t)}{1 - g(\delta_t)} \end{aligned}$$

A similar equation holds for the orthonormal columns in the DFT matrix, except that for them, there is an additional integer multiple of  $2\pi$ , as shown in (11).

$$\begin{aligned} \alpha[\theta_t] \alpha^*[\theta_t + (l/P) + \delta_t] &= \sum_k g(k\theta_t) g^*(k\theta_t) \cdot g(k\delta_t) \\ &= \sum_k g(k\delta_t) = \frac{1 - g(l + P\delta_t)}{1 - g(\delta_t)} \end{aligned} \quad (11)$$

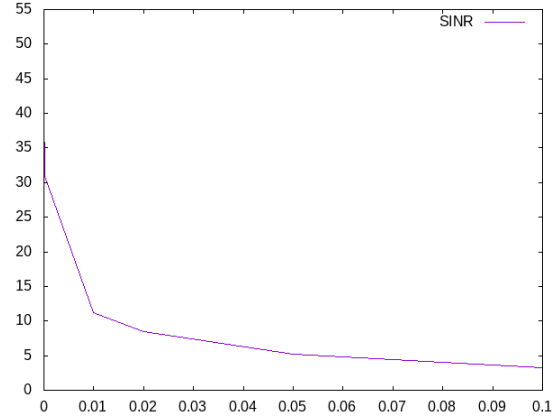


Fig. 4. Variation of SINR with the error term

Fig. 5. Optimal Offset Calculation

- 1: **procedure** FINDBESTPHASE( $L, \beta[], a[], P$ )  $\triangleright$  Cluster size,  $\beta$  values, angles, number of antenna
- 2: Sort  $a[]$  in decreasing order of  $\beta$
- 3:  $\Psi \leftarrow 0$
- 4: **for** each angle in the cluster  $j$  **do**  $\psi^* \leftarrow 100$  ;
- 5:  $r \leftarrow \frac{\beta[j]}{\sum_m \beta_m}$
- 6: **for** each antenna slot  $0 \leq k < P$  **do**
- 7:  $\phi \leftarrow |a[] - k/P|$
- 8: **if**  $\phi < \psi^*$  **then**
- 9:  $\psi^* \leftarrow \psi$
- 10: **end if**
- 11: **end for**  $\Psi \leftarrow \Psi * (1 - r) + \psi^* * r$
- 12: **end for**
- 13: **end procedure**

The chart in Figure 4 shows the impact of the error on the SINR. As is expected, the chart is asymptotic with a cutoff at approximately 1% of error.

2) *Handling multiple clusters:* We now consider the problem of handling multiple cluster elements, each having an individual pair of arrival and departure angles  $\langle \theta_r^i, \theta_t^i, \beta_r^i \rangle$ . We wish to continue to use the offsetting approach from III-B. To do this, we need to find a single common pair of shifts  $\psi_r, \psi_t$  which works for all  $L$  clusters. Assuming that all the cluster angles fall within the range  $[2\pi \frac{-N/2-1}{N}, 2\pi \frac{-N/2+1}{N}]$ , this can be done by find  $p_l, q_l$  for each pair, so that the corresponding residual is mapped into a common 'slot' and then choosing a phase shift for that slot applicable to all the pairs. How this works is shown in the procedure given in Figure 5.

#### IV. ESTIMATING CHANNEL DIRECTIONS USING MACHINE LEARNING

From the discussion in Section III, we have established that given a good estimate of the angles of arrival and departure of the mm-wave channel, it is possible to construct beam-shaping precoders/decoders for the mm-wave channel. However, the challenges of doing blind estimation of these parameters using conventional search techniques is well-established [39,40]. Because the boresight is very tight, a

detailed search (typically heirarchical) is required to get a good *first fix*, after which iterative improvement is possible. This requires multiple sweeps of the channel using by both transmitter and receiver and can considerably delay the channel lock time. Of course, if one of the two are mobile, then the problem is even more challenging, because the channel angles change rapidly with the environment.

Machine learning has been suggested in a multitude of works [28,30,31] as a suitable technique by which to get a quick estimate of the  $\langle \text{AoA}, \text{AoD} \rangle$  pairs for a cluster of mm-wave double-directional paths. As has been identified in the literature, the key to the successful use of ML is to find the optimal fingerprint to use as the input to the ML algorithm. Since ML algorithms operate on the basis of training, we have to find some parameter which has a constant mapping to the AoA/AoD pairs, within the highly variable mm-wave environment; if we can't, then the entire basis for an ML based algorithm is moot.

#### A. Applicability of Machine-Learning techniques to the problem of beam selection

Machine learning techniques operate in two stages [41]. The first *learning* phase, the ML engine is fed a sequence of training data; each data-set consists of a two parts; the data domain identifier (also called the finger print), the action and the outcome. The task of the ML-engine is to develop an association between the fingerprint, the set of actions and the outcome, which is implicitly stored in its model. In the second *application* phase, the ML-engine is fed a real set of data, consisting of the identifiers; for each such identifier, it uses its internal model to suggest the action which will give a good outcome.

We can write this as a formal model, where the identifier  $i$  is taken from a space  $\mathcal{I}$ , the action  $a$  is from the set  $\mathcal{A}$  and the outcome  $o$  is from the space  $\mathcal{O}$ . The physical process is represented as a function  $f$  given by  $f() : \mathcal{I} \times \mathcal{A} \rightarrow \mathcal{O}$ . We assume that the outcome space  $\mathcal{O}$  consists of a small number outcomes  $\{o_1, o_2, \dots, o_K\}$ , where each  $o_k$  is an open ball in  $\mathcal{O}$ . If  $f()$  is an onto-map, we can then assume that the domain  $\mathcal{I} \times \mathcal{A}$  is a union of individual sets  $\Gamma_1 = f^{-1}(o_1), \Gamma_2 = f^{-1}(o_2), \dots$ . The purpose of Machine Learning, is to determine the structure of sets  $\Gamma_k$ , based on a certain number of observations or training inputs  $v_j^t = f(i_j^t)$ , without explicitly knowing the structure of  $f()$ . We further assume that  $f()$  changes slowly enough with time, so that for any given period  $|t \dots t + \Delta|$ , the change in  $f()$  due to time is either negligible or can be linearly interpolated. We recall that this is one of the reasons why ML cannot be used in the standard sub-6Ghz MIMO case, since the channel changes rapidly on a frame-to-frame basis.

Even with the above quasi-stationarity condition, there are three possible structures for  $\bigcup_k \Gamma_k$ , of which only one is amenable to the Machine Learning space. In the first case, each  $\Gamma_k$  is an open ball in  $\mathcal{I} \times \mathcal{A}$  and  $f_k : \Gamma_k \rightarrow o_k$  the restriction of  $f()$  to the  $k^{th}$  set in  $\mathcal{I} \times \mathcal{O}$  is a continuous map. This is the simplest case to consider, and does not typically require an ML based solution. The second case is when

the sets  $\Gamma_k$  are  $\epsilon$ -dense in each other i.e.  $\forall x \in \Gamma_k, \delta \exists y \in \Gamma_{j \neq k}$  such that  $|y - x| \leq \delta$ . As  $\epsilon \rightarrow 0$ , the function  $f()$  becomes chaotic, because of the impossibility of measuring  $x$  finely enough in the training period. The case where Machine Learning works is when  $\Gamma_k$  is suitably complex, but has some kind of internal structure which can be determined as the outcome of the training process.

#### B. Fingerprinting the mm-wave channel

Choosing the domain  $\mathcal{I}$  of the ML algorithm is equivalent to the choice of the fingerprint and it is crucial to our approach. In signal-processing literature, research has focussed on two or three categories of fingerprints for the mm-wave channel. The first is *RSSI fingerprinting*, typically measured simultaneously by multiple receivers or radio-heads. The second is *multi-path* fingerprinting, where the focus is on multi-path characteristics (such as Power Delay Profile (PDP)) rather than signal strength. The last is the respective positions of the transmitter and receiver. Other innovative techniques utilize metrics such as the channel covariance metric or other measures which attempt to capture some aspect of the channel multipath profile.

In this paper, we use the location of the UE with respect to the gNodeB as the fingerprint. We argue that this choice meets our criteria as listed previously. It is well known that the relation between location and beam-angles is extremely non-linear because of the nature of the mm-wave propagation path; detailed simulation models based on ray tracing techniques and empirical validation thereof seem to confirm this [5,42]. The validity of the second criterion is possible to demonstrate by considering the extreme linearity of the mm-wave channel and the tight angular spread; it is very likely that the signal quality at a particular location and direction are very tightly correlated, since a small change in angular spread would give rise to a very large variation in the RSSI readings.

However there are some associated issues with the choice of location as the input parameter. The UE location is not directly observable by the gNodeB, but has to be reported by the UE (unlike, for example, RSSI, which is directly measured at the gNodeB). This implies that there has to be a separately established channel for communicating the location-beam mapping between the UE and gNodeB. For example, assuming that the UE knows its own position, the gNodeB can broadcast the table of optimal beams with respect to the different locations within the coverage area separately and allow the UE to select the ones that match its own current location. Further, directly using location as a finger-printing technique means that the input domain is very large. We would like to decrease the granularity of location, without choosing arbitrary boundaries. We shall subsequently demonstrate this in our simulation results in section V-A below.

#### C. Choice and design of the Machine Learning Algorithm

In this paper, we have chosen a deep learning based model based on supervisory learning. Supervised learning-based

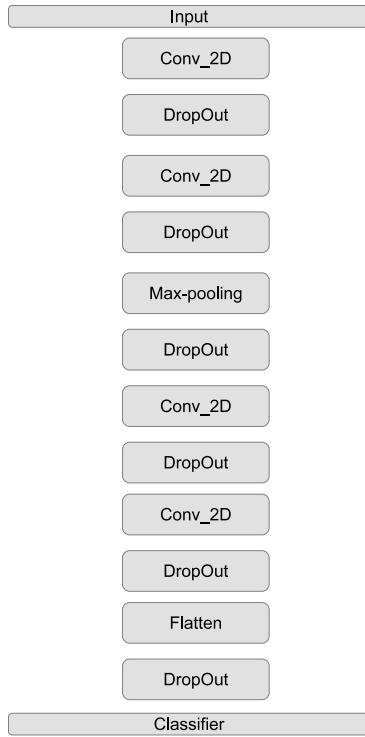


Fig. 6. Deep Neural Network for beam prediction

model is used which take ray tracing related information as input and labeled optimal beam pair indices as output. For solving optimal beam pair as a classification problem, we can quantize the angles using vector or scalar quantization. If the latter is used, the angles can be quantized into four indices according to their dynamic ranges in the training set. These indices can be eventually converted to a single label for traditional classification. The quantized values are then mapped into the range  $[1 \dots M]$ , where  $M$  is the number of known beams.

A deep neural network (DNN) with  $L$  layers describes a mapping of an input vector to an output vector through  $L$  iterative processing steps. This mapping depends not only on the output vector from the previous layer but also on a set of parameters (i.e., weights and biases). In a DNN, many units are deployed in each hidden layer, and the output can be generated based on the output of these units with the aids of activation functions. The activation function introduces a non-linearity which gives advantage of stacking multiple layers on top of each other. In this paper we have used a Convolutional DNN framework as shown in Fig. 6. Here, in the input layer will take the training data.

As can be seen from Figure 6, our DNN has 11 hidden layers between the input and the two output layers. As is well known in the literature [43], the presence of the convolutional and pooling layers helps the CNN focus on local correlations between the inputs avoiding, among other issues, the over-training problem. [44] provides an excellent introduction to the theory of convolutional deep neural networks for the interested reader.

The neural network that we use is trained using supervisory learning, using a labeled training data set i.e., a set of input-

Parameter Name	Parameter Value
batch size	32
epochs	100
validation fraction	1
learning rate	0.0001
optimizer	SGD (lr=learning rate, momentum=0.9)
regression loss	mean squared error
regression metric	mse
classification loss	categorical cross_entropy
classification metric	accuracy

TABLE I: DNN Hyper-parameters

output vector pairs. A certain loss function, such as square error or cross entropy, must be established for the network to produce a value that is close to the expected one as much as possible. The goal of the training process is to minimize the loss with respect to the parameters. The number of samples of training data taken for computing this loss at each time interval is called as batch size. The back-propagation algorithm has been proposed as an efficient method for training the network with optimization algorithms such as Stochastic Gradient Descent. Although the trained network performs well in the training data, this network may perform poorly in the testing process because of over-fitting. To avoid overfitting and to achieve favorable results in training and testing data schemes such as early stopping, regularization, and dropout have been used. The table I shows the top-level parameters of the D-CNN we have used.

#### D. Simulating against real-life data

There is a lack of authentic set of data from real communication systems or prototype platforms in actual physical environments. So far, simulations results [30,32,34] prove that the recently proposed DL-based communication algorithms demonstrate a competitive performance. However due to the lack of standardized data, benchmarking of the performance is a real challenge.

For the purpose of this work, we took input data as generated using ray-tracing based on a scenario based on region of Rosslyn, Virginia, from the authors of [30]<sup>1</sup>. The method used by the authors is as follows. The Ray tracing (RT) area of study is a rectangle of approximately  $337 \times 202$ , with a road on the north side and a second road perpendicular to it from the south, intersecting it at the top. A transmitter is located at the RSU on Kent Street, approximately at the middle of the area and receivers are placed on top of 10 receivers. The ray-tracing outputs are periodically stored as *snapshots* (or scenes) with a sampling interval  $T_{sam}$ . A total of  $N$  scenes are combined to form an *episode*. After this processing, we obtain a dataset, containing 116 episodes, with each episode having 50 scenes per episode. The episodes are sliced into  $N_{sce}$  individual scenes of a fixed duration  $\tau_{epi}$ , to improve the scene diversity and reduce computational load. Within each episode, we store information based on the transmitters, receivers and Mobile Object

<sup>1</sup>We acknowledge the help given us by the authors in this regard



Fig. 7. Grid of positions

(MOBJs). This includes dimensions of all MOBJs, mappings between transmitters/receivers and MOBJs, coordinates of the RT study area and number  $L$  of rays per transmitter / receiver pair. After the ray-tracing, the scene is updated with the information related to each transmitter/receiver pair  $(m, n)$ . These are the average time of arrival  $\tau_{m,n}$ , total transmitted and received powers  $P_{m,n}^t, P_{m,n}^r$ , and for the  $l$ th ray  $1 \leq l \leq M$ , the channel  $\Gamma_{l,m,n}$  characteristic associated with that ray, comprising of the complex channel gain, time of arrival and AoD, AoA angles respectively.

$$\Gamma_{l,m,n} = \langle \beta^{l,m,n}, \tau^{l,m,n}, \phi_{l,m,n}^D, \phi_{l,m,n}^A, \theta_{l,m,n}^D, \theta_{l,m,n}^A \rangle \quad (12)$$

In the equation (12)  $\phi$  and  $\theta$  correspond to the azimuth and elevation for departure and arrival respectively. As shown in the section III-B, we are at this point only interested in the azimuth angles  $\theta^A, \theta^D$ .

### E. Preparation of the data-set

To test out our ML algorithm, we use the individual data sets as described above, along with the location fingerprint to train the model for prediction the channel parameters for each new input fingerprint. The data-generation model assumes that the communication channel between the transmitter and receiver for sharing location/beam-parameters is pre-established. The position and identity information is then represented as a matrix. In order to quantize the location data, the coverage area with area  $23 \times 250$  sq.m, broken into a grid with resolution of  $1 \times 1$  sq.m. . This can be represented by a matrix  $Q_s$  of dimension  $23 \times 250$  grid points for each scene  $s$ . The training data baseline is generated by ray-tracing. Each grid point is occupied by either a receiver or an interferor of known height. This is represented in the matrix by a negative or positive value at each grid point. A negative element in  $Q_s$  indicates that the corresponding location is occupied (even partially) by an obstruction. The magnitude of this negative value indicates the obstructor's height. A positive integer value  $r$  at a given position indicates that the  $r$ th receiver is in that position in  $Q_s$ . 0 denotes the position is not occupied. Figure 7 illustrates an example where the receiver is blue and the surrounding obstructions are yellow. When training classifiers, one can then conveniently represent the labels with one-hot encoding to facilitate training neural networks. We pose the beam-selection as a classification task

in which the target output is the best beam pair index  $\hat{i}$ . The input features correspond to the matrix described as  $Q_{s,r}$ , a modified version of  $Q_s$  for each receiver  $r$ , assuming a value +1 for all  $Q_s$  elements corresponding to the target receiver  $r$ , while all other receivers in the given scene  $s$  are represented with -1 (instead of their original positive values in  $Q_s$ ). For our particular case, we have a total of 5300 entries, out of which a third are used for testing. For each receiver that is part of a given data-set a classification example is obtained, leading to a total of 41,023 examples for training and test. Among the examples, there is LOS in 25,174 cases and NLOS in 15,849. Transmitter and receivers had  $4 \times 4$  uniform planar antenna arrays (UPA), such that  $N_t = N_r = 16$ . From all the possible beams the authors have identified  $M = 61$  classes (optimum beam pairs), within which the search is to take place.

## V. SIMULATION RESULTS AND CONCLUSION

Using the dataset generated as described in IV-D and IV-E, we have tested out our deep-learning algorithm. The algorithm was used to predict appropriate beams for a total of 13000 random sample-points. For each sample-points, we took the top  $N \ll M$  best beams as predicted by the Deep Learning algorithm and compared it with the results of the ray tracing exercise for the associated location. It should be noted that the total number of mapped beams  $M = 61$  are based on a clustering exercise and hence, not tuned to the model. By reducing these, we may get better prediction results, but then the relative coarseness of beam selection will give rise to higher deviation between the predicted beam parameters and the actual parameters based on ray-tracing. These issues will be considered in more detail in a subsequent paper.

### A. Simulation results

The Figure 8 captures the beam prediction accuracy based on the  $N$  best beams predicted. If we take only the best beam i.e.  $N = 1$ , then the accuracy of prediction is of the order of 64%. But if we consider the top  $N = 3$  beams in terms of accuracy then the chances of prediction is approx. 85%. Hence, instead of best prediction if we can have top 3 prediction than it will help use in improving the beam prediction capability. The search space is significantly reduced in this manner. Clearly, even choosing the top  $M = 5$  beams offers a vast performance improvement over a brute-force search for each location over the full search space of 61 possible beams. As discussed above, the selection of the beam dictionary and broadcasting this dictionary (and associated location mapping) is an area of open research.

### B. Does diversity improve performance?

A strong reason to go to the edge would be if using multiple transmitters instead of one improve per-location beam prediction accuracy. Given that the cumulative prediction accuracy for a given transmitter seems to saturate after 3 best beams, it may make more sense to take, say the top 2 beams from 4 sites, rather than using more beams from a given

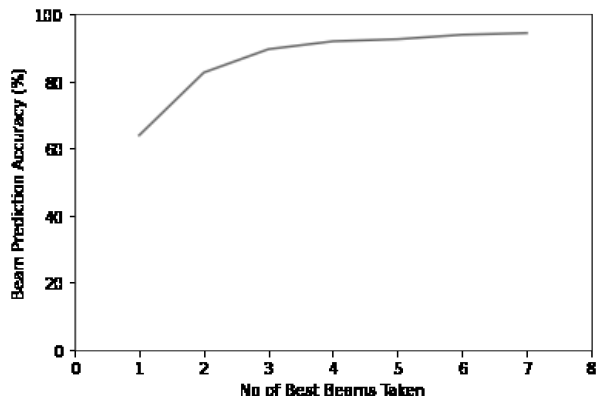


Fig. 8. Success of predicting beam-sets

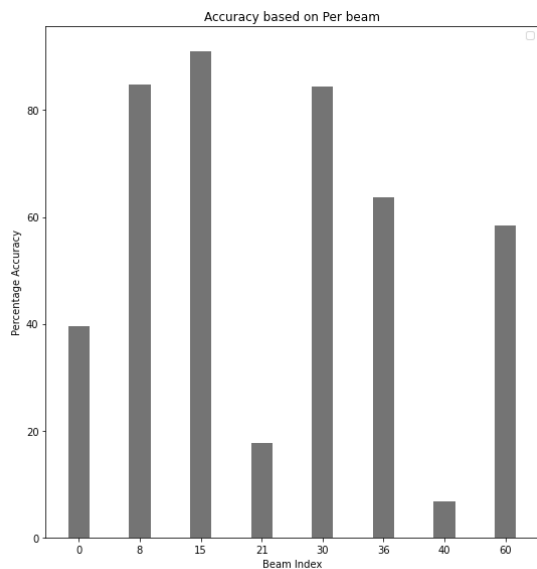


Fig. 9. Error rate over different beams

site. However, this only works if the prediction accuracy of a given location with respect to different transmitters is uncorrelated with each other. There is not much information or study on the nature of the error in DNN type of models; i.e. whether the error is truly random or whether there is correlation between errors. Obviously, if there is correlation between the different sites in a multi-site gNodeB, then our diversity gains will be limited. To study this, we looked at the prediction error of a given DNN indexed across locations for within a single data-set (Figure 9). Since the beams are mapped onto locations, we can use the beam-index as a proxy for location data. The preliminary investigation shows that prediction accuracy varies as a function of beam index (and hence location) for the same training data. In future work, we shall analyze the source of this error, given that the training data was more or less evenly distributed over all locations and the terrain chosen was uniform. Prima facie, we can say that using multiple transmitters from different sites should give us a diversity gain, as opposed to the idea of running a single transmitter.

### C. Machine Learning at the edge - Deployment considerations

The majority of the existing literature focus on centralized ML/DL (as shown in Figure 10a) whose goal is to improve the communication performance assuming a well-trained ML model as well as full access to a global dataset. It also assumes massive amount of storage and computing power is available. However, the development of the 5G network and the new model for RAN development, provides the possibility of implementing the beamforming algorithm, both the training and the application part right at the edge. The new generation of mobile platforms shall offer the possibility of executing these algorithms in a containerized environment on a general purpose (GPU equipped) hardware platform on the same platform in which the physical layer is running. The advantages are clearly, manifold. The algorithm has immediate access to all the measurements available to the gNB and can provide near instantaneous feedback to the beam-former in terms of the optimal beam-shaping matrices. On the other hand, the availability of processing power at the edge is limited and thus, we need to come up with a way to fit our ML (especially the training part of it) into the limited resources available. The DNN that we have implemented for our beam prediction algorithm has a total of 934235 separate parameters and consumes a fair amount of processing power during the training phase. Being able to fit it into the restricted resources available would be a challenge. In our simulations, we have plotted the GPU loading and memory utilization for the training algorithm, as shown in Figure 11. The data has been generated by Google Collab. As can be seen, each run of the training algorithm consumes nearly the full available GPU and associated memory resources.

The third and possibly most practical architecture is a hybrid model, whereby the training is implemented in a centralized location (with access to large computing power) and the actual inference engines are present on the wireless edge. This is the model we have used in this paper, leveraging the Mobile Edge architecture proposed in the latest O-RAN specifications [45] (Figure 10b). In this model, the computational load problem is replaced by the problem of communicating large amounts of data. It is notable that the training models have to be separate for each edge site, since the fingerprint is highly site specific; hence the training outcome has to be individual in nature.

### D. Conclusions

In this paper, we have studied the mm-wave beamforming problem and implemented a simple solution using supervisory learning. We have verified our algorithm against a ray-tracing implementation and seen that we get about 90% accuracy in predicting appropriate beam parameters. We have shown how we can use multiple RRHs working in tandem to increase the prediction accuracy and how a hybrid edge-cloud model can be used to implement this scheme. Machine Learning is a fairly young discipline, with very recent applications to the field of wireless channel management. In terms of the mm-wave channel, the literature is very new. There is a lack

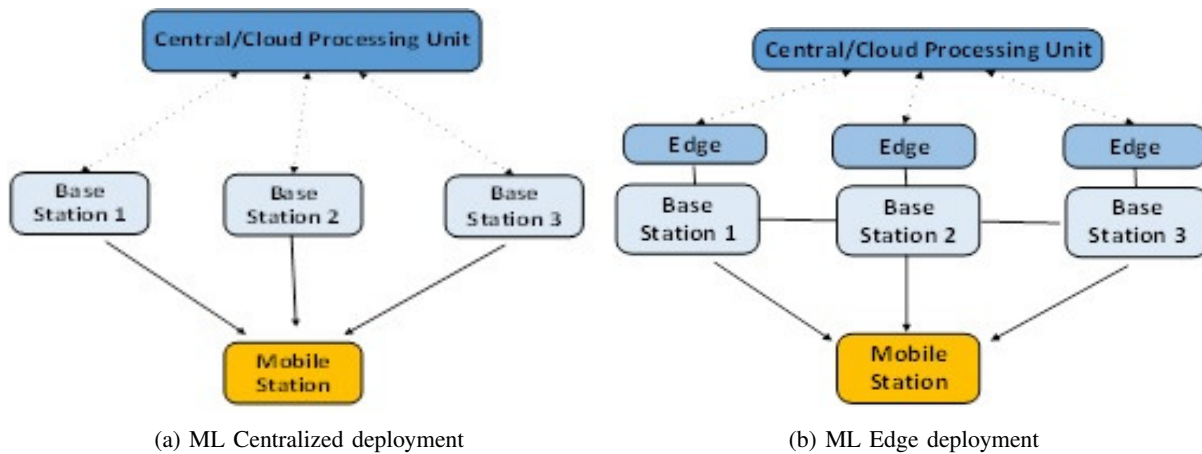
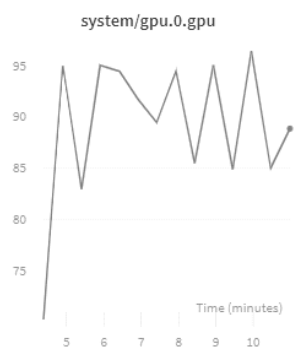
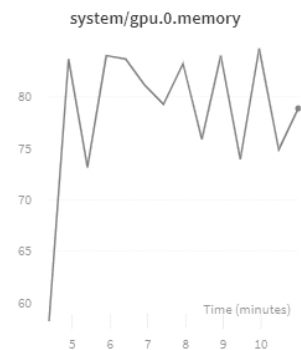


Fig. 10. Deployment strategies for ML based beam forming algorithms



(a) GPU utilization



(b) Memory utilization during training

Fig. 11. GPU computing and resource utilization during training

of simulation data, especially given that ML is a very data-hungry discipline and the testing of new ML models require lots of observations. Further, there are practical challenges in ML deployment; ML algorithms use a lot of processing power, especially during training and this is constrained in a wireless network, where digital processing consumes the maximum amount of CPU. Hence, we believe that the focus should be on using simple ML algorithms in an inventive manner.

## REFERENCES

- [1] M. Giordani and M. Zorzi, "Improved user tracking in 5g millimeter wave mobile networks via refinement operations," in *2017 16th Annual Mediterranean Ad Hoc Networking Workshop (Med-Hoc-Net)*, June 2017, pp. 1–8.
- [2] M. Polese, M. Giordani, M. Mezzavilla, S. Rangan, and M. Zorzi, "Improved handover through dual connectivity in 5g mmwave mobile networks," *IEEE Journal on Selected Areas in Communications*, , , September, vol. 35, no. 9, pp. 2069–2084, 2017.
- [3] S. Schwarz, C. Mehlh rner, and M. Rupp, "Calculation of the spatial preprocessing and link adaptation feedback for 3gpp umts/lte,," in *Proceedings of the 6th conference on Wireless advanced (WiAD)*. IEEE, .. 2010, pp. 1–6.
- [4] M. Giordani, M. Mezzavilla, A. Dhananjay, S. Rangan, and M. Zorzi, "Channel dynamics and snr tracking in millimeter wave cellular systems,," in *Proceedings of the 22th European Wireless Conference*, 2016, pp. 1–8.
- [5] Q. C. Li, G. Wu, and T. S. Rappaport, "Channel model for millimeter-wave communications based on geometry statistics," in *2014 IEEE Globecom Workshops (GC Wkshps)*, Dec 2014, pp. 427–432.
- [6] T. N. et al., "Ieee 802.11ad: directional 60 ghz communication for multi-gigabit-per-second wi-fi [invited paper],," *IEEE Communications Magazine*, vol. 52, no. 12, pp. 132–141, December 2014.
- [7] J. Wang, "Beam codebook based beamforming protocol for multi-gbps millimeter-wave wpan systems," *IEEE Journal on Selected Areas in Communications*, vol. 27, no. 8, pp. 1390–1399, October 2009.
- [8] R. Santosa, B.-S. Lee, C. K. Yeo, and T. M. Lim, "Distributed neighbor discovery in ad hoc networks using directional antennas,," in *The Sixth IEEE International Conference on Computer and Information Technology*, September, 2006.
- [9] C. Jeong, J. Park, and H. Yu, "Random access in millimeter-wave beamforming cellular networks: issues and approaches," *IEEE Communications Magazine*, vol. 53, no. 1, pp. 180–185, January 2015.
- [10] C. N. B. et al., "Directional cell discovery in millimeter wave cellular networks," *IEEE Transactions on Wireless Communications*, , , , December, vol. 14, no. 12, pp. 6664–6678, 2015.
- [11] —, "Directional initial access for millimeter wave cellular systems," in *in 49th Asilomar Conference on Signals, Systems and Computers*. IEEE, 2015.
- [12] V. Desai, L. Krzymien, P. Sartori, W. Xiao, A. Soong, and A. Alkhatieb, "Initial beamforming for mmwave communications,," in *in 48th Asilomar Conference on Signals, Systems and Computers*, 2014, pp. 1926?, 1930.
- [13] L. Wei, Q. Li, and G. Wu, "Exhaustive, iterative and hybrid initial access techniques in mmwave communications,," in *in 2017 IEEE Wireless Communications and Networking Conference (WCNC)*. IEEE, 2017.
- [14] J. Choi, "Beam selection in mm-wave multiuser mimo systems using compressive sensing," *IEEE Transactions on Communications*, , , , August, vol. 63, no. 8, pp. 2936–2947, 2015.
- [15] A. S. Cacciapuoti, "Mobility-aware user association for 5g mmwave networks," *IEEE Access*, , ?21 507,, vol. 5, pp. 21–497, 2017.

- [16] J. Palacios, D. D. Donno, and J. Widmer, "Tracking mm-wave channel dynamics: Fast beam training strategies under mobility," in *IEEE Conference on Computer Communications (INFOCOM)*. IEEE, 2017.
- [17] K. Chandra, R. V. Prasad, I. G. Niemegeers, and A. R. Biswas, "Adaptive beamwidth selection for contention based access periods in millimeter wave w lans," in *IEEE 11th Consumer Communications and Networking Conference (CCNC)*. IEEE, 2014.
- [18] A. Alkhateeb, Y. H. Nam, M. S. Rahman, J. Zhang, and R. W. Heath, "Initial beam association in millimeter wave cellular systems: analysis and design insights," *IEEE Transactions on Wireless Communications*, , , May, vol. 16, no. 5, pp. 2807–2821, 2017.
- [19] Y. Li, J. Luo, M. Castaneda, R. Stirling-Gallacher, W. Xu, and G. Caire, "On the beamformed broadcast signaling for millimeter wave cell discovery: Performance analysis and design insight," *arXiv preprint arXiv:1709.08483*, 2017.
- [20] S. articleDorner, S. Cammerer, J. Hoydis, and S. ten Brink., "Deep learning-based communication over the air," <https://arxiv.org/abs/1707.03384>.
- [21] U. Challita, L. Dong, and W. Saad, "Proactive resource management in lte-u systems: A deep learning perspective," <https://arxiv.org/abs/1702.07031>, 2017.
- [22] R. C. Daniels, C. M. Caramanis, and R. W. Heath, "Adaptation in convolutionally coded mimo-ofdm wireless systems through supervised learning and snr ordering," *IEEE Trans. Veh. Technol.*, , , January, vol. 59, no. 1, pp. 114–126, 2010.
- [23] S. K. Pulliyakode and S. Kalyani, "Reinforcement learning techniques for outer loop link adaptation in 4g/5g systems," <https://arxiv.org/abs/1708.00994>.
- [24] A. Fehske, J. Gaeddert, and J. H. Reed, "A new approach to signal classification using spectral correlation and neural networks," in *Proc. IEEE Int. Symp. New Frontiers in Dynamic Spectrum Access Networks (DYSpan)*, 2005.
- [25] E. E. Azzouz and A. K. Nandi, "Modulation recognition using artificial neural networks," in *Proc. Automatic Modulation Recognition of Communication Signals*, 1996.
- [26] M. Ibukahla, J. Sombria, F. Castanie, and N. J. Bershad, "Neural networks for modeling nonlinear memoryless communication channels," *IEEE Trans. Commun.*, , , July, vol. 45, no. 7, pp. 768–771, 1997.
- [27] A. Mazin, M. Elkourdi, and R. D. Gitlin, "Accelerating beam sweeping in mmwave standalone 5g new radios using recurrent neural networks," in *2018 IEEE Vehicular Technology Conference (VTC)*, 2018.
- [28] —, "Comparative performance analysis of beam sweeping using a deep neural net and random starting point in mmwave 5g new radio," in *2018 9th IEEE Annual Ubiquitous Computing, Electronic and Mobile communication conference (UEMCON)*, 2018.
- [29] V. Va, J. Choi, T. Shimizu, G. Bansal, and R. W. Heath, "Inverse multipath fingerprinting for millimeter wave v2i beam alignment," *IEEE Transactions on Vehicular Technology*, vol. 67, no. 5, pp. 4042–4058, May 2018.
- [30] A. Klautau, P. Batista, N. Gonzalez-Prelcic, Y. Wang, and R. W. H. Jr, "5g mimo data for machine learning: Application to beam-selection using deep learning," in *Proc of the information theory and application workshop, February*, 2018.
- [31] V. Shimizu, G. Bansal, and R. W. Heath, "Online learning for position-aided millimeter wave beam training," *January*, 2019.
- [32] V. Va, T. Shimizu, G. Bansal, and R. W. Heath, "Position-aided millimeter wave v2i beam alignment: A learning-to-rank approach," in *2017 IEEE 28th Annual International Symposium on Personal, Indoor, and Mobile Radio Communications (PIMRC)*, Oct 2017, pp. 1–5.
- [33] Y. Wang, M. Narasimha, and R. H. Jr., "Mmwave beam prediction with situational awareness: A machine learning approach," *January*, 2019.
- [34] A. Alkhateeb, S. Alex, P. Varkey, Y. Li, Q. Qu, and D. Tujkovic, "Deep learning coordinated beamforming for highly-mobile millimeter wave systems," *February*, 2019.
- [35] Y. Wang, M. Narasimha, and R. W. H. Jr, "Mmwave beam prediction with situational awareness: A machine learning approach," in <https://arxiv.org/abs/1805.08912>, June, 2018.
- [36] A. Alkhateeb, S. Alex, P. Varkey, Y. Li, Q. Qu, and D. Tujkovic, "Deep learning coordinated beamforming for highly-mobile millimeter wave systems," *IEEE Access*, , –37 348, June, vol. 6, pp. 37–328, 2018.
- [37] W. Roh, J. Seol, J. Park, B. Lee, J. Lee, Y. Kim, J. Cho, K. Cheun, and F. Aryanfar, "Millimeter-wave beamforming as an enabling technology for 5g cellular communications: theoretical feasibility and prototype results," *IEEE Communications Magazine*, vol. 52, no. 2, pp. 106–113, February 2014.
- [38] M. R. Akdeniz, Y. Liu, M. K. Samimi, S. Sun, S. Rangan, T. S. Rappaport, and E. Erkip, "Millimeter wave channel modeling and cellular capacity evaluation," *IEEE Journal on Selected Areas in Communications*, vol. 32, no. 6, pp. 1164–1179, June 2014.
- [39] P. Schniter and A. Sayeed, "Channel estimation and precoder design for millimeter-wave communications: The sparse way," in *2014 48th Asilomar Conference on Signals, Systems and Computers*, Nov 2014, pp. 273–277.
- [40] R. W. Heath, N. Gonzalez-Prelcic, S. Rangan, W. Roh, and A. M. Sayeed, "An overview of signal processing techniques for millimeter wave mimo systems," *IEEE Journal of Selected Topics in Signal Processing*, vol. 10, no. 3, pp. 436–453, April 2016.
- [41] J. Hertz, A. Krogh, and R. G. Palmer, *Introduction to the Theory of Neural Computation*. Westview Press, September 1990.
- [42] M. Di Renzo, "Stochastic geometry modeling and analysis of multi-tier millimeter wave cellular networks," *IEEE Transactions on Wireless Communications*, vol. 14, no. 9, pp. 5038–5057, Sep. 2015.
- [43] T. N. Sainath, A. Mohamed, B. Kingsbury, and B. Ramabhadran, "Deep convolutional neural networks for lvcsr," in *2013 IEEE International Conference on Acoustics, Speech and Signal Processing*, 2013, pp. 8614–8618.
- [44] M. D. Zeiler and R. Fergus, "Visualizing and understanding convolutional networks," in *European conference on computer vision*. Springer, 2014, pp. 818–833.
- [45] L. M. Larsen, A. Checko, and H. L. Christiansen, "A survey of the functional splits proposed for 5g mobile crosshaul networks," *IEEE Communications Surveys & Tutorials*, vol. 21, no. 1, pp. 146–172, 2018.